UNIVERSITY OF GAZİANTEP

GRADUATE SCHOOL OF

NATURAL & APPLIED SCIENCES

INVESTIGATION OF STRUCTURAL AND OPTICAL PROPERTIES OF SPRAYED CuS FILMS

M. Sc. THESIS

IN

ENGINEERING PHYSICS

BY

MAHMUD TEKİN

JUNE 2011

Investigation of Structural and Optical Properties of Sprayed CuS Films

M. Sc. Thesis

in

Engineering Physics

University of Gaziantep

Supervisor

Assoc. Prof. Dr. Metin BEDİR

by

Mahmud TEKİN

June 2011

T.C.
UNIVERSITY OF GAZİANTEP
GRADUATE SCHOOL OF
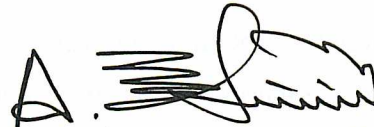NATURAL & APPLIED SCIENCES
NAME OF THE DEPARTMENT

Name of the thesis: Investigation of Structural and Optical Properties of Sprayed
CuS Films.
Name of the student: Mahmud TEKİN
Exam date:08.06.2011

Approval of the Graduate School of Natural and Applied Sciences

Prof. Dr. Ramazan KOÇ
Director

I certify that this thesis satisfies all the requirements as a thesis for the degree of
Master of Science/Doctor of Philosophy.

Prof. Dr. A. Necmeddin YAZICI
Head of Department

This is to certify that we have read this thesis and that in our consensus/majority
opinion it is fully adequate, in scope and quality, as a thesis for the degree of Master
of Science.

Assoc.Prof.Dr. Metin BEDİR
Supervisor
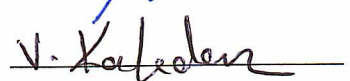
Examining Committee Members   Signature

Title and Name-surname

Assoc.Prof.Dr.Mustafa ÖZTAŞ

Assoc.Prof.Dr.Metin BEDİR

Assit.Prof.Dr. E.Vural KAFADAR

ABSTRACT

INVESTIGATION OF STRUCTURAL AND OPTICAL PROPERTIES OF SPRAYED CuS FILMS

TEKİN, Mahmud

M.Sc. in Engineering Physics

Supervisor: Assoc. Prof. Dr. Metin BEDİR

June 2011, 92 pages

In this study, semiconducting CuS films were developed under different $CuCI_2$ ratios by using spraying pyrolysis method and their crystal structure and optical properties were widely investigated by using different techniques.

The crystal structure of the CuS samples were determined from x-ray diffraction peaks and the thickness of the sprayed CuS thin film samples were calculated by using weighing method. The optical properties of semiconducting CuS thin films were investigated from optical absorption coefficient data using double beam visible spectrofotometer. By using these data band gap energies of the semiconducting CuS thin films were determined. And also the variations of the properties of the samples as a function of the annealing conditions were investigated.

Key Words: spray pyrolysis method, CuS thin film, structural and optical properties, annealing.

ÖZET

PÜSKÜRTME YÖNTEMİYLE ELDE EDİLEN CuS FİLMLERİN YAPISAL ve OPTİKSEL ÖZELLİKLERİNİN İNCELENMESİ

TEKİN, Mahmud

Yüksek Lisans Tezi, Fizik Mühendisliği

Danışman: Doç. Dr. Metin BEDİR

Haziran 2011, 92 Sayfa

Bu çalışmada püskürtme yöntemiyle cam alt tabanlar üzerine farklı $CuCl_2$ oranlarında CuS ince filmler büyütülüp, onların yapısal ve optiksel özellikleri farklı teknikler kullanılarak derinlemesine araştırılmıştır.

CuS film numunelerinin kristal yapıları x-ışınımı difraktometresinden elde edilen pikler kullanılarak incelenmiş ve ince film numunelerinin kalınlıkları ağırlık yöntemiyle hesaplanmıştır. Yarı iletken CuS ince filmlerin optiksel özellikleri çift ışıklı olup görünür bölgede çalışan spekrometreden elde edilen optiksel soğurma katsayıları analiziyle araştırılmıştır. Bu veriler kullanılarak yarı iletken CuS ince filmlerin enerji band değerleri hesaplanmıştır. Bunun yanı sıra, CuS numunelerinin özelliklerinin tavlama ile değişimi araştırılmıştır.

Anahtar Kelimeler: püskürtme yöntemi, CuS ince film, yapısal ve optiksel özellikler, tavlama.

ACKNOWLEDGEMENT

During the writing of this thesis, the author received many helps from people to whom he would like to thank. First of all I would like to thank my supervisor Assoc. Prof. Dr. Metin BEDİR for all his help and advice during the preparation of this thesis.

Secondly, I wish to thank Assoc. Prof. Dr. Mustafa ÖZTAŞ. I have benefited from the aid and advice of him during the writing and preparation of this thesis. I would like to thank my gratitude to the research assistances and other personnel at the Department of Engineering Physics for their kind help and friendships.

Especially, I would like to give my special thanks to my wife Hatice whose patient love enabled me to complete this work.

CONTENTS

LIST OF FIGURES

LIST OF TABLES

CHAPTER 1
LITERATURE SURVEY

1.1 Introduction

Due to their structural, electrical and optical properties, copper sulfides ($Cu_{2-x}S$, x=0-1) thin films are widely used as semiconductor and/or absorber materials with application in electronics, photovoltaic cells, and tubular solar collectors. Among these, CuS (covellite) thin films are known to exhibit metalikle electrical conductivity and to posses near-ideal solar control characteristics. All these make of CuS thin films deposited onto different substrates (glass, polymers) promising materials for either electric and electronic devices or radiation control coatings (filters) [1].

1.2 Historical Survey

Different techniques have been used for the CuS thin films deposition, such as chemical bath deposition, [4], photochemical deposition, [5], metal organic chemical vapor deposition, [6], doctor Blade, [7] and spray pyrolysis deposition [8]. Spray pyrolysis is a simple and low-cost technique used to deposit thin films at nanoscale, mesoscale or microscale. The present study focuses on the formation (nucleation/growth) of CuS thin films by SPD, correlating the crystalline structure (crystallite size) with the surface morphology (average grain size). These depend on the precursor solution composition and deposition parameters.

Covellite, the stoichiometric copper-poor phase (66,46% Cu), is a green-black crystalline solid with a special hexagonal crystalline structure, consisting of layers of planar CuS_3 triangles, containing Cu^{2+} and S^{2-} ions, surrounded (above and below) by CuS_4 tetrahedral arrangements of Cu^+ and S^{2-} ions. The Cu-S distances in tricoordinated Cu_2^+ are 2.19 Å, while in tetrahedral Cu^+ are 2.31 Å. Two-third of the sulfur species are S_2^{2-} anions and one-third are S^{2-} ions [2]. The lattice parameters of various crystalline types of covellite are: a = 3.768-3.796 Å and c = 16.27-16.382 Å [3]. The crystalline structure correlated with the surface morphology gives important information on the ratio of the nucleation and growth reactions. These strongly

depend on the deposition technique and parameters. Different techniques have been used for the CuS thin films deposition, such as chemical bath deposition, photochemical deposition, metal organic chemical vapor deposition, doctor Blade, and spray pyrolysis deposition. Spray pyrolysis is a simple and low-cost technique used to deposit thin films at nano-, meso- or microscale [4].

CdS/CuS and CuS/CdS thin films were deposited on glass substrates at room temperature by chemical bath deposition technique. The structural characterization was done using Philips PW 1800 X-ray diffractometer (XRD) while the absorption coefficient (α) together with the band gap were determined using the absorbance and transmission measurement from a Unico uv-2102 PC spectrophotometer, at normal incidence of light in the wavelength range of 200-1000nm. The results of the optical characterization of CdS/CuS heterojunction thin films were compared with optical properties of binary thin films of CdS and CuS. The results show a clear deviation in the optical properties of the stacks of CdS/CuS thin films from the individual binary films that make up the stacks. The plot of $(\alpha h v)^2$ against $(h v)$ showed that the materials have direct band gap values 1.70, 2.00, 2.10 and 2.30 eV for CuS, CuS/CdS, CdS/CuS and CdS respectively [9].

Nanocrystalline Cu_xS (x=1,2) thin films were deposited by asynchronous-pulse ultrasonic spray pyrolysis (APUSP) technique on glass from $CuCl_2$ and thiourea at relatively low temperature without any complexing agent. The deposited films chemically close to CuS were found to be polycrystalline phases, while the Cu_2S films were a mixture of amorphous and polycrystalline as well. The crystalline phase of particles was highly depended on the molar ratio of thiourea to $CuCl_2$ and the pyrolysis temperature. The growth of Cu_xS thin films was controlled successfully by the improved APUSP method. Characterization of the films has been carried out using X-ray diffraction (XRD), scanning electron microscopy (SEM), X-ray photoelectron spectroscopy (XPS) and Raman spectroscopy. XRD and XPS analysis showed stoichiometric Cu_xS (covellite CuS and chalcolite Cu_2S). Raman shifts of the films were measured at 474 cm^{-1} (CuS) and 472 cm^{-1} (Cu_2S) [10].

Spray pyrolysis deposition of CuS thin films using aqueous solutions containing $CuCl_2.2H_2O$, thiourea and cationic surfactant, is presented. The transmission and reflexion spectra in the VIS-NIR region of such films are recorded.

The electrical resistances and photosensitivities, as well as optical energy band gap (2.2 eV) are also determined. The spray pyrolyzed CuS films show p-type conductivity [11].

Cu$_x$S (x = 1,2) thin films have recently received considerable attention due to numerous technological applications in achievement of solar cells [12-19], in photothermal conversion of solar energy (as solar absorber coatings) [17,20-23], as selective radiation filters on architectural windows (for solar control in the warm climates) [1,13-17], as electroconductive coatings deposited on organic polymers [18-26]. At room temperature, Cu$_x$S in the bulk form is known to exist in five stable phases: chalcocite (orthorhombic Cu$_2$S), djurleite (Cu$_{1,95}$S), digenite (Cu$_{1,8}$S), anilite (Cu$_{1,75}$S) and covellite, (CuS) [12,27]. Mixed phases are also known in the intermediate compositions [32]. Various techniques have been employed to prepare Cu$_x$S thin films such as vacuum evaporation, chemical bath deposition, spray pyrolysis (for x higher than 1), sputtering etc.

The spray pyrolysis method has been used widely to deposit other sulfides films (predominantly CdS, but also PbS, Sn$_2$S$_3$, SnS) because it is relatively cheap and simple. The work reports, possibly for the first time to our knowledge, spray pyrolysis deposition of CuS thin films. It also presents the basic optical, electrical and photoelectrical properties of these films.

CuS (hcp) with different morphologies was produced using a transient solid-state reaction by the direct flow of electricity through solids, containing 1:1 molar ratio of Cu:S powders, in a high vacuum system for different lengths of time. X-ray diffraction (XRD), selected area electron diffraction (SAED), and scanning and transmission electron microscopies (SEM and TEM) specified that the products were nanostructured CuS flowers, and nanostructured CuS composing of nanoparticles with different orientations, controlled by the length of time. Raman vibrations were detected at 474.5 cm^{-1}, and photoluminescent (PL) emissions at 347.5nm. Both the XRD and SAED patterns are in accordance with those obtained by the corresponding simulations [38].

Copper sulfides are the IB-VIA compounds having different phases, such as covellite (CuS), anilite (Cu$_7$S$_4$), digenite (Cu$_{1,8}$S), djurleite (Cu$_{31}$S$_{16}$) and chalcocite (Cu$_2$S) [39]. CuS is one of semiconducting materials, which have a wide variety of

applications: solar radiation absorbers [40], optical filters [41] and cathode materials in lithium rechargeable batteries [40]. It has semiconducting or metallic conducting property, and transforms into a superconductor at 1.6 K [42]. There are different methods used to produce this compound: hydrothermal and solvothermal synthesis [40-43], microwave radiation [44], a polyol route and solid-state reaction [45]. To the best of our knowledge, there have been no reports on the production of CuS by a transient solid-state method. Thus, it is very interesting to produce nanostructured CuS flowers, and nanostructured CuS of nanoparticles with different orientations by direct flowing of electricity through a copper-sulfur solid mixture in vacuum. This method is novel, efficient and rapid.

The structural changes in Cu_xS films have been monitored by X-ray diffraction and correlated to the chemical changes taking place on the Cu_xS surface, the latter monitored by XPS. The results show: evaporated Cu_xS films contained chalcocite, free copper phases, and probably a third phase (of sulfur); resistivity is related to the amounts of free Cu and S in the film; air heat treatments converted chalcocite to Cu deficient phases and resulted in the disappearance of the sulfide and predominance of $CuSO_4 \cdot nH_2O$ and CuO; argon heat treatment tended to react Cu and S to form Cu_xS; Cd is detected on the surface of Cu_xS deposited onto CdS and is significantly increased in amount by heat treatments. These results can be related to chemical processes occurring on Cu_xS/CdS and Cu_xS/(Zn,Cd)S solar cells. For the CdS cell, oxides and sulfates of Cu and Cd are found on the Cu_xS surface and the sulfates are enhanced by the heat treatment in moist air. CuO and $CuSO_4$ are formed in the absence of Cd, and dominate the Cu_xS surface [46].

The controlled synthesis of copper sulfide (CuS) nanoplate-based architectures in different solvents has been realized at low cost by simply reaction of $Cu(NO_3)_2.3H_2O$ and S under solvothermal conditions without the use of any template. X-ray diffraction (XRD), scanning electron microscopy (SEM), transmission electron microscopy (TEM), UV/VIS spectrometer and fluorescence measurement were used to characterize the products. The products were all in hexagonal phase with high crystallinity and the morphology was significantly influenced by the solvents. The CuS products synthesized in dimethylformamide (DMF) were nanoplates and the samples prepared in ethanol were flower-like morphology composed of large numbers of nanoplates, but those synthesized in

ethylene glycol (EG) were CuS architectures with high symmetry made up of several nanoplates arranged in a certain mode. The optical properties were investigated and the growth mechanisms of these CuS crystals were also proposed [47].

In the field of materials science and synthesis chemistry, semiconductor-related optical materials with controlled crystal structures, shapes and sizes have drawn extensive attention owing to their structurally and dimensionally dependent physical properties and potential applications. As a family of optical and electrical materials, copper-sulfur system has received particular attention since the discovery of its photovoltaic properties [48,49]. In this system, there are a number of Cu_xS compounds such as chalcocite (Cu_2S), djurleite ($Cu_{1.9375}S$), anilite ($Cu_{1.75}S$), and covellite (CuS), among which, Cu_2S is of great interes due to its small band gap, high ionic conduction, and photovoltaic capabilities [50].

The assembly of one-dimensional (1D) materials is an important goal of contemporary materials science [51]. Cu_2S nanorods have also successfully been fabricated using the vapor-solid reaction method [52], which provides a mild way to obtain high quality 1D nanostructure materials without undergoing the tedious catalytic synthesis processes at high temperatures [53-55]. In order to understand the electric and chemical properties as well as the size dependence of the electronic structure of Cu_2S nanorods, we have performed polarization dependent X-ray absorption spectroscopy (XAS) measurements at Cu L3-edge of nanorods with different diameters. The studies of the molecular orbitals have greatly benefited from XAS. XAS can be used to determine the geometric structures of molecules and clusters under different sample preparation and surface structures [56].

Recently, the fabrication of uniform hollow spheres with dimensions from nanometer to micrometer has become a focus in nanoscience and nanotechnology because of their broad range of applications in photonic crystals, catalysts, coatings, composites, fillers and the protection of light-sensitive components, especially in delivery vehicle systems for the controlled release of drugs, cosmetics, inks, and dyes [57]. A variety of chemical and physicochemical methods have been employed to produce hollow spheres composed of metal, polymer, carbon and inorganic materials. However, there has been only little progress in the template-free technique for fabrication of hollow spheres. Sulfides of copper are a particularly interesting

class of metal sulfides because of their ability to form various stoichiometrical products. Many methods have been developed for the preparation of sulfides of copper nanoparticles. However, no hollow sulfides of copper spheres are reported in the literature. Herein, we reported a novel template-free route to fabricate hollow $Cu_{2-x}S$ micron spheres at the ambient conditions [58].

Flexible electronics has already found a variety of commercial and defence applications such as in wearable computers, electrotextiles [59], large area sensors, and displays on flexible substrates [60,61]. One of the key challenges to the successful development of such applications is the development of electrical conductors, which can be fabricated on flexible and, ideally, stretchable, substrates and sustain large mechanical strain. Recently, we reported on depositing semiconductor materials, such as CdS, CdSe, PbS and semiconducting metallic Cu_7S_4 films on large flexible substrates and threads at temperatures close to room temperature [62,63]. We also reported on the photovoltaic effect in polycrystalline semiconductor CdS cells deposited on view foils [64] and threads [65]. Such solar cells could provide a renewable energy source (energy harvesting) for electrotextiles and for "sensitive skin". In this Letter, we report on the structural and electrical properties of Cu_7S_4 films deposited on viewfoil. Cu_7S_4 thin films were deposited by the chemical bath technique described in [66]. By adjusting the concentrations of Cu ions and Na_2Sn poly sulphide and using multiple deposition cycles, we obtained Cu_7S_4 films with the resistivity as low as 100% per square. The deposited thin films exhibited excellent adhesion to the polymeric substrate. The films were deposited at temperatures 60-70^{0}C. Because of low deposition temperatures, we were also able to use a variety of flexible materials, including viewfoils, cloths, and threads. We covered the areas up to several tens of square inches. The layer thickness was measured as 2.5 mm using both the "AlphaStep" profilometer on the selectively etched Cu_7S_4 layer and by the Atomic Force Microscope (AFM) on the cross-section of the structures.

CuS, $Cu_{0.6}Zn_{0.4}S$ and ZnS thin films were grown by successive ionic layer adsorption and reaction(SILAR) method on glass substrates at room temperature. The annealing temperature effect on the crystal structure, optical band gap and the light effect on the electrical properties of these films have been investigated. Scanning electron microscope (SEM) and X-ray diffraction (XRD) techniques were

used for the investigation of structural properties of films. The SEM and XRD studies showed that the films are covered well with glass substrates and exhibit polycrystalline characterization. Using the absorption measurements, the band gap energies for CuS, $Cu_{0.6}Zn_{0.4}S$ and ZnS thin films were found as 2.03, 2.14 and 3.92 eV at room temperature, respectively. The two-point-probe method was used for the investigation of electrical properties of films and it was found that the current increase with increasing light intensity and increasing rate in illuminated 500W cm^{-2} films was greater than in others. There is an important increasing in the current values of the CuS and $Cu_{0.6}Zn_{0.4}S$ films which have annealed at $400^{0}C$. But the annealed ZnS thin film has less current values than the as-grown film. This is the first study which led to deposition of the CuZnS thin films by using the SILAR method [67].

$Cu_{x}S$ thin films with a wide range of sheet resistances (R) and optical transmittance (T%), indicating different composition x, have been obtained from chemical baths constituted from copper(II) chloride, triethanolamine and thiourea at appropriate pH (10-12). Depending on the deposition parameters, a range of combination of R=30Ω to 1 MΩ and T% (500 nm)$\approx$l to 65 and a range of colour of reflected daylight (golden yellow, purple, blue, green, etc) can be obtained. The films have been found to be stable with respect to electrical and optical properties on storage under ambient. Various possible large area applications such as in architectural glazing, photothermal and photovoltaic conversions are discussed [68].

CHAPTER 2
CRYSTAL STRUCTURE

2.1 Introduction

Since interatomic distances are in the region of 100-300 pm or 1-3 Å, microscopy using visible light (wavelength λ ca.300-700 nm) is not applicable. In 1912, Max von Laue showed that crystal are based on a three dimensional lattice which scatters radiation with a wavelength in the vicinity of interatomic distances, i.e. X-rays with λ=50-300 pm. The process by which this radiation, without changing its wavelength, is converted through interference by the lattice to a vast number of observable "reflections" with characteristic directions in space is X-ray diffraction. The method by which the directions and the intensities of these reflections are measured, and the ordering of the atoms in the crystal deduced from them, is called X-ray structure analysis [69].

To solve a crystal structure means to determine the precise spatial arrangements of all of the atoms in a chemical compound in the crystal state. This knowledge gives a chemist access to a large range of information, including connectivity, conformation, and accurate bond lengths and angles. In addition, it implies the stoichiometry, the density, the symmetry and the three dimensional packing of the atoms in the solid.

2.1.1 Crystals

The economically most important semiconductors have a relatively simple atomic arrangement and are highly symmetric. The symmetry of the atomic arrangement is the basis for the classification of the various crystal structures. Using group theory, basic and important conclusions can be drawn about the physical properties of the crystal, such as its elastic and electronic properties. The presence of highly symmetric planes is obvious from the crystal shape of the minerals and their cleavage behavior [70]. In crystalline solids such as semiconductors, the individual

atoms form a periodic array of sites called the crystal lattice. The world crystal originates from the Greek word kristallos, which stand for ice. For a solid such as Si, the equilibrium state is reached, when the environment viewed from each atom looks exactly the same. The resulting periodocity is very important in describing some basic properties of semiconductors. In amorphous semiconductors such as amorphous Si, the long range periodicity does not exist anymore.

Polycrystalline semiconductors consist of grains of finite size that are structurally perfect. The grain boundaries are a lattice defect. Amorphous semiconductors are disordered on the atomic scale [71].

2.1.2 Crystal Lattice

The crystal lattice is typically described by a translation or Bravais lattice. The French natural scientist A. Bravais was the first to classify all possible three-dimensional lattices according to their symmetry. A Bravais lattice consist of an array of points, which can be generated by the translation vector R given by

$$N_i a_i \qquad\qquad (2.1)$$

Here, N_i denotes integer numbers and a_i the three primitive vector of the lattice, which are three vectors not all in the same plane. Each lattice point represents an atom or group of atoms. The arrangement of these lattice points acquires a well-defined symmetry. The lattice point can be located at the center of an atom or of a group of atoms, but this is not required. The volume defined by the three vectors ai is called the primitive unit cell. By translating this unit cell through all the vector in a Bravais lattice, all of space is fulled without any overlap between this unit cell or any voids between them.

There is no unique way of choosing a primitive cell for a given Bravais lattice. An important primitive unit cell is the Wigner-Seitz cell, which exhibits the full symmetry of the Bravais lattice. It is defined by the region around the lattice point, which is closer to that point than to any other lattice point. It is usually constructed by (i) drawing lines connecting the lattice point to all others in the lattice, (ii) bisecting each line with a plane, and (iii) taking the smallest polyhedron bounded by these planes. An example of a Wigner-Seitz cell in two dimensions is shown by the shaded area in Fig. 2.1 [71].
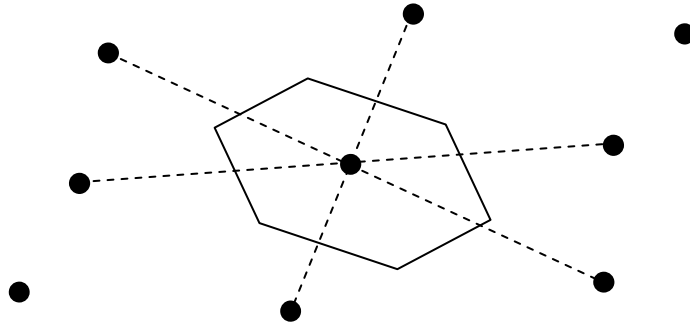
Figure 2.1 The Wigner-Seitz cell (shaded area) for a two-dimensional Bravais lattice. In two dimensions the Wigner-Seitz cell is always a hexagon unless the lattice is rectangular.

The atoms in a crystal are said to be located in a space lattice. If each atom in the lattice is replaced by a point, each such point is referred to as a (three dimensional) lattice array. The properties of the crystal as a whole can be considered in terms of identical unit cells of which it is composed. The three sides of a unit cell, which are called the crystallographic axes, are chosen to have directions such that they pass regularly through the lattice points associated with like atoms; each unit cell encloses one lattice point [72].

The simple hexagonal lattice is obtained by stacking two-dimensional triangular nets shown in the left panel of Fig. 2.2, which are spanned by two primitive vectors of equal length making an angle of 60^0, directly above each other. The direction of stacking defines the c-axis. The first two primitive vectors generate the triangular lattice in the x-y plane, while the third stacks the planes a distance c above one another. The number of nearest neighbors with distance a is six, while there are only two nearest neighbors at distance c. The Wigner-Seitz cell of the simple hexagonal lattice shown in two dimensions by the shaded area in the right panel of Fig. 2.2 is a prism with regular hexagon as the base [71].
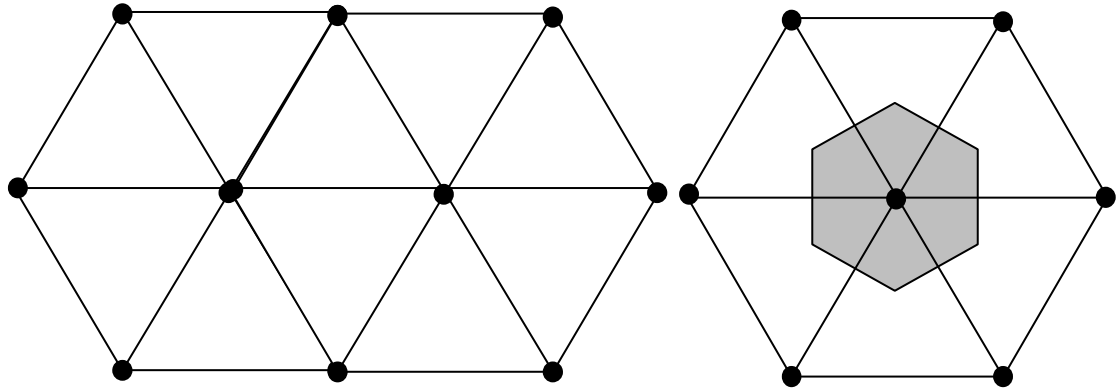
Figure 2.2 The simple hexagonal lattice (left) and its Wigner-Seitz cell (right) indicated by the shaded area in two dimensions.

2.1.2.1 Periodic Structures of Solids

Classification of solids can be based on atomic arrangement, binding energy, physical and chemical properties, energy bands or the geometrical aspects of the crystalline structure. A solid substance with its atoms held apart at equilibrium spacing, but with no long-range periodicity in atom location in its structure is an amorphous solid. Examples of amorphous solids are glass and same types of plastic. They are sometimes described as supercooled liquids because their molecules are arranged in a random manner somewhat as in the liquid state. For example, glass is commonly made from silicon dioxide or quartz sand, which has a crystalline structure. When the sand is melted and the liquid is cooled rapidly enough to avoid crystallization, an amorphous solid called a glass is formed. Amorphous solids do not show a sharp phase change from solid to liquid at a definite melting point, but rather soften gradually when they are heated.

In another class, the atoms or group of atoms in the solid are arranged in a regular order. These solids are referred to as the crystalline solids. The crystalline solids can be further divided into two categories: the single-crystalline and polycrystalline solids. In a single-crystalline solid, the regular order extends over the entire crystal. In a polycrystalline solid, however, the regular order exists only over a small region of the crystal, with grain size ranging from a few hundred angstroms to a few centimeters. A polycrystalline solid contains many of these small single-crystalline regions surrounded by the grain boundaries. Distinction between these

two classes of solids-amorphous and crystalline- can be made through the use of X-ray or electron diffraction techniques [73].

2.1.2.2 Cubic Lattice

The crystal structure of a material or the arrangement of atoms within a given type of crystal structure can be described in terms of its unit cell. The cubic (or isometric) crystal system is a crystal system where the unit cell is in the shape of a cube. This is one of the most common and simplest shapes found in crystals and minerals.

There are three main varieties of these crystals, called simple cubic (sc), body-centered cubic (bcc), and face-centered cubic (fcc), plus a number of other variants listed below. The simple cubic structure has an atom located at each corner of the unit cell. The body-centered cubic lattice has an additional atom at the center of the cube, and the face-centered cubic unit cell has atoms at the eight corners and centered on the six faces. Note that although the unit cell in these crystals is conventionally taken to be a cube, the primitive unit cell often is not. This is related to the fact that in most cubic crystal systems, there is more than one atom per cubic unit cell.
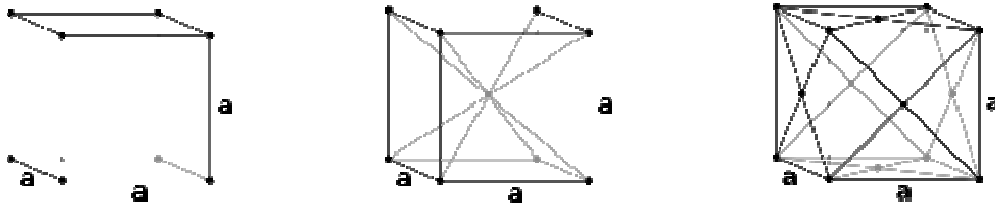
Figure 2.3 Simple cubic lattice, body-centered cubic lattice, face-centered cubic lattice.

2.1.2.3 Diamond Structure

Group IV elementary semiconductors such as Si and Ge crystallize in the same structure as diamond. All these materials exhibit tetrahedral bonding form by sp-hybridization so that each atom is surrounded by four nearest neighbors located at the four corners of a regular tetrahedron. This configuration of neighbors cannot be represented by any of the basic cubic lattices. It can, however, be fulfilled by two fcc

lattices with a basis as shown in figure. The number of nearest neighbors is four and the number of atoms per primitive cell two [71].
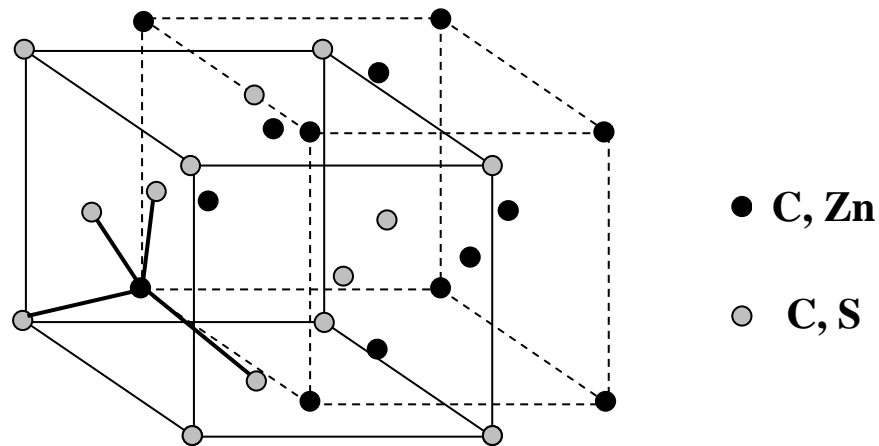
Figure 2.4 The diamond crystal structure. If two fcc lattices contain different atoms (black and gray circles), the zincblende structure is generated. One tetrahedral group is indicated by the thick lines.

2.2 Energy Bands for Solids

An important parameter in the band theory is the Fermi level, the top of the available electron energy levels at low temperatures. The position of the Fermi level with the relation to the conduction band is a crucial factor in determining electrical properties.

A useful way to visualize the difference between conductors, insulators and semiconductors is to plot the available energies for electrons in the materials. Instead of having discrete energies as in the case of free atoms, the available energy states form bands. Crucial to the conduction process is whether or not there are electrons in the conduction band. In insulators the electrons in the valence band are separated by a large gap from the conduction band, in conductors like metals the valence band overlaps the conduction band, and in semiconductors there is a small enough gap between the valence and conduction bands that thermal or other excitations can bridge the gap as shown in Fig. 2.5.

13

Energy of Electrons

Conduction Band

Large energy gap
between valence
band and
conduction bands.

Valence Band

a. Insulator

Conduction Band

Valence Band

b. Semiconductor

Fermi
level

Conduction Band

Valence Band
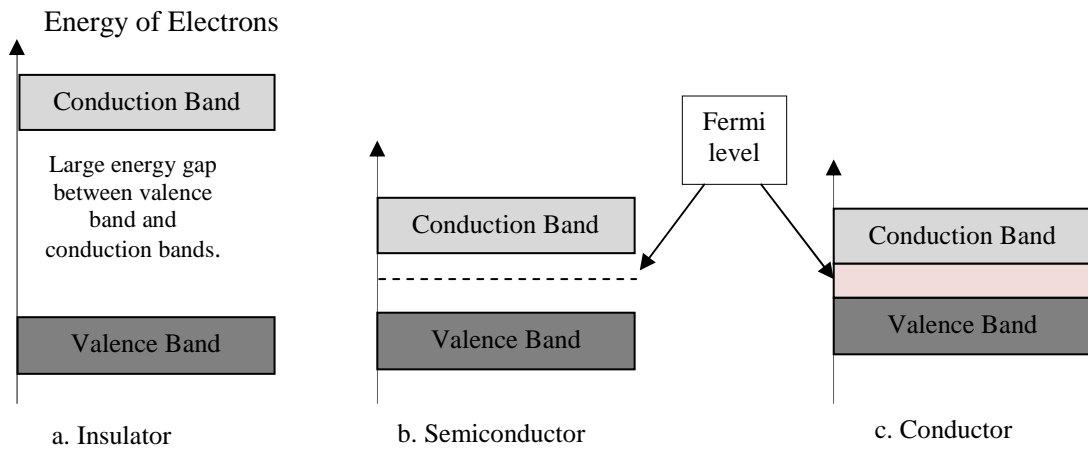
c. Conductor

Figure 2.5 Energy band diagrams of the conductors, insulators and semiconductors.

The difference in energy between the top of the valence band and the bottom of the conduction band is called the energy gap or the band gap of the semiconductor as shown in Fig. 2.5. This is perhaps the most important single parameter describing semiconductor behavior and it tells us a great deal about the semiconductor. Silicon has a band gap of about 1.1 eV at room-temperature (semiconductor band gaps usually vary just a little with temperature) so an electron must gain 1.1 eV of energy to cross the band gap [74].

CHAPTER 3
SEMICONDUCTOR

3.1 Introduction

Semiconductors are an important class of material both for industrial use and for scientific study. Over the last two decades, semiconductors have come to be used in a wide range of electronic devices, such as transistors, switching devices, voltage regulators, photocells, and photodetectors. The rapid growth of the semiconductor industry has stimulated the demands for better material understanding and material quality. The technology of crystal growth developed during this period has made it possible to produce crystals of exceedingly high purity and crystal perfection. In the meantime, the list of semiconductor materials has expanded steadily. The availability of new and good-quality materials and the demand for a better understanding of material properties have prompted scientists to make concerted efforts in many directions. The interplay between technology and science in this area has been one of the most fruitful and rewarding experiences in human endeavor [75].

However, there is a much larger number of semiconductors available today, and more and more III-V and II-VI compound semiconductors find their application. Within the last decade we have seen GaAs high-electron mobility transistors used in satellite dishes as well as cellular phones and GaAs/Al_xGa_{1-x}As laser diodes in compact disc players. A blue laser based on ZnSe was realized some years ago. Very recently a blue light-emitting laser diode based on GaN was developed. Finally, solar cells are fabricated from semiconducting materials. Their use in houses and consumer products is steadily increasing [71].

3.1.1 Theory

Materials that combine some of the electrical characteristics of conductors with those of insulators are known as semiconductors. Common types of semiconductor material are silicon, germanium, selenium and gallium. In the pure state, these materials may have relatively few free electrons to permit the flow of

electric current. However, it is possible to add foreign atoms (called impurity atoms) to the semiconductor material in order to modify the properties of the semiconductor and allow it to conduct electricity.

It should be recalled that an atom contains both negative charge carriers (electrons) and positive charge carriers (protons). Electrons each carry a single unit of negative electric charge while protons each exhibit a single unit of positive electric charge. Since atoms normally contain an equal number of electrons and protons, the net charge present will be zero. For example, if an atom has eleven electrons, it will also contain eleven protons. The end result is that the negative charge of the electrons will be exactly balanced by the positive charge of protons.

Electrons are in constant motion as they orbit around the nucleus of the atom. Electron orbits are organized into shells. The maximum number of electrons present in the first shell is two, in the second shell eight, and in the third, fourth and fifth shells it is 18, 32 and 50, respectively. In electronics, only the shell furthermost from the nucleus of an atom is important. It is important to note that the movement of electrons between atoms only involves those present in the outer valence shell.
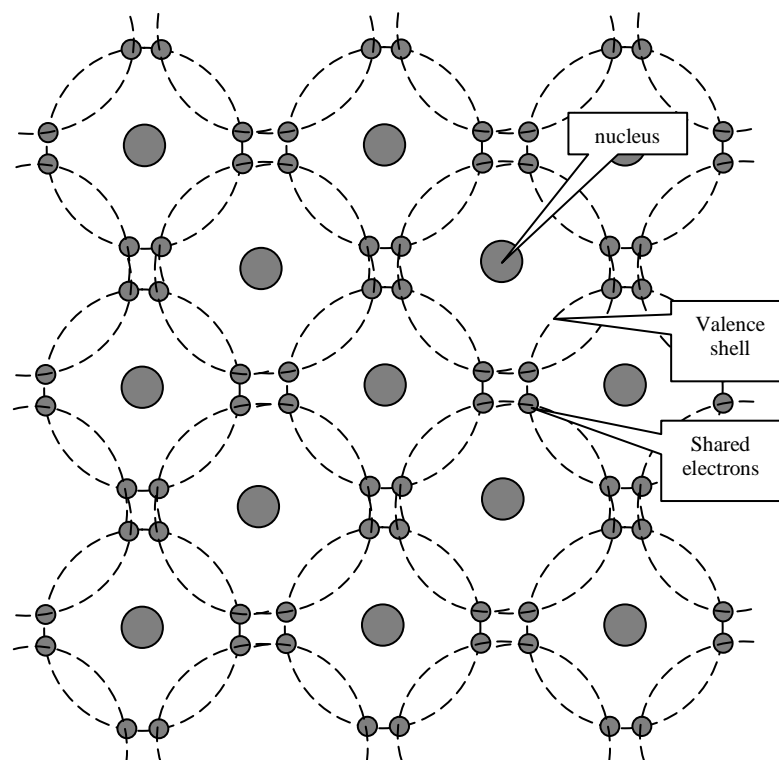
Figure 3.1 Regular lattice structure of a pure semiconductor material.

16

If the valence shell contains the maximum number of electrons possible the electrons are rigidly bonded together and the material has the properties of an insulator. If, however, the valence shell does not have its full complement of electrons, the electrons can be easily detached from their orbital bonds, and the material has the properties associated with an electrical conductor.

In its pure state, silicon is an insulator because the covalent bonding rigidly holds all of the electrons leaving no free (easily loosened) electrons conduct current. If, however, an atom of a different element (i.e. an impurity) is introduced that has five electrons in its valence shell, a surplus electron will be present (see Fig. 3.2). These free electrons become available for use as charge carriers and they can be made to move through the lattice by applying an external potential difference to the material.
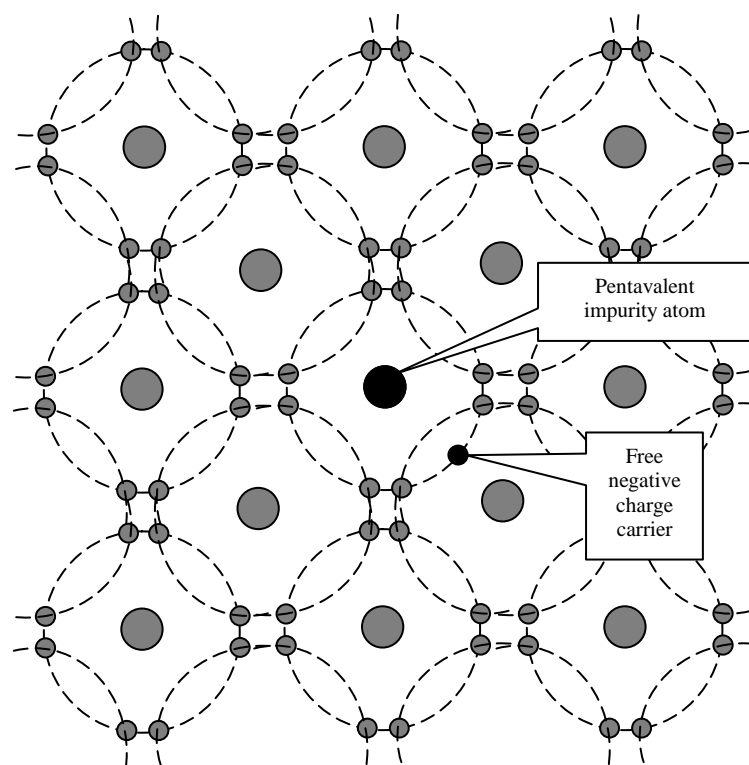
Figure 3.2 Effect of introducing a pentavalent impurity.

Similarly, if the impurity element introduced into the pure silicon lattice has three electrons in its valence shell, the absence of the fourth electron needed for proper covalent bonding will produce a number of spaces into which electrons can fit (see Fig. 3.3). These gaps are referred to as holes. Once again, current will flow when an external potential difference is applied to the material.

Regardless of whether the impurity element produces surplus electrons or holes, the material will no longer behave as an insulator; neither will it have the properties that it normally associate with a metallic conductor. Instead, it is called the material a semiconductor that the term simply indicates that the substance is no longer a good insulator nor a good conductor but has the properties of something between the two. Examples of semiconductors include germanium (Ge) and silicon (Si).
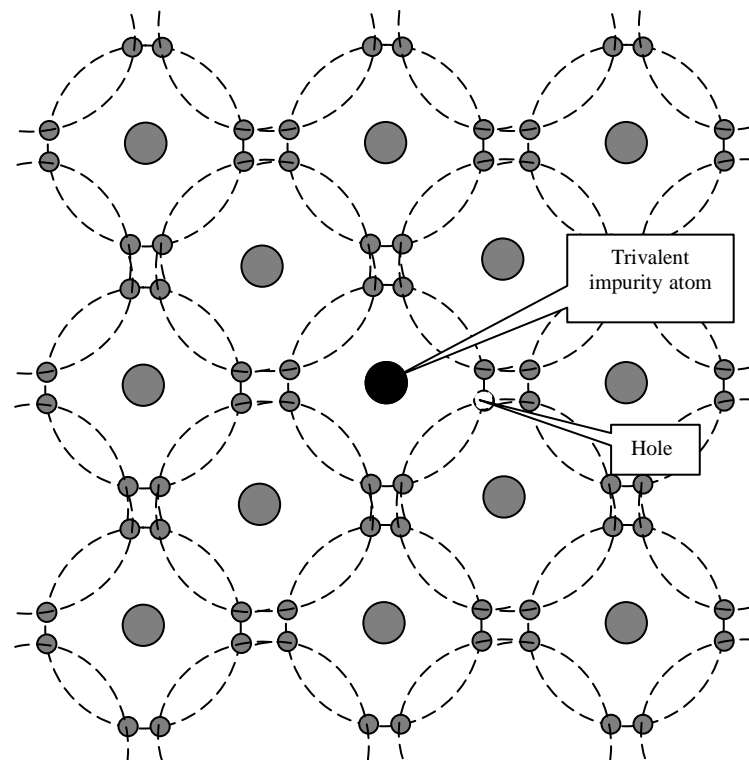
Figure 3.3 Effect of introducing a trivalent impurity.

The process of introducing an atom of another (impurity) element into the lattice of an otherwise pure material is called doping. When the pure material is doped with an impurity with five electrons in its valence shell (i.e. a pentavalent impurity) it will become an n-type (i.e. negative type) material. If, however, the pure material is doped with an impurity having three electrons in its valence shell (i.e. a trivalent impurity) it will become p-type material (i.e. positive type). N-type semiconductor material contains an excess of negative charge carriers, and p-type semiconductor material contains an excess of positive charge carriers [76].

3.1.2 Semiconductor Fundamentals

An intrinsic semiconductor also called an undoped semiconductor or i-type semiconductor is a pure semiconductor without any significant dopant species

present. The properties of the material determine the number of charge carriers itself instead of the amount of impurities. In intrinsic semiconductors the number of electrons and the number of holes are equal. Intrinsic semiconductors are essentially pure semiconductor material. The semiconductor material structure should contain no impurity atoms. Elemental and compound semiconductors can be intrinsic semiconductors.

An extrinsic semiconductor can be formed from an intrinsic semiconductor by added impurity atoms to the crystal in a process known as doping. By taking as an example Silicon; since Silicon belongs to group IV of the periodic table, it has for valence electrons. In the crystal form, each atom shares an electron with neighboring atom. In this state it is an intrinsic semiconductor. B, Al, In, Ga all has three electrons in the valence band.

3.1.3 Semiconductor Materials

Semiconductor materials have physical characteristics that are totally different from those of metals. Whereas metals conduct electricity at all temperatures, semiconductors conduct well at some temperatures and poorly at others.

Semiconductors are covalent solids, that is the most important being silicon and germanium in Group IV of the periodic table. Others may form semiconductor compounds where two or more elements form covalent bonds, such as gallium (Group III) and arsenic (Group V), which combine to form gallium arsenide.

- Elemental semiconductors
    - Silicon
    - Germanium
    - Selenium

- Semiconducting compounds
    - Gallium arsenide (GaAs)
    - Gallium arsenide-phosphide (FaAsP)
    - Indium phosphide (InP)

Germanium is an elemental semiconductor that was used to fabricate the first transistors and solid state devices. But, because it is difficult to process and inhibits device performance, it is rarely used now.

The other elemental semiconductor, silicon, is used in approximately 90 percent of the chips fabricated. Silicon's popularity can be attributed to its abundance in nature and retention of good electrical properties, even at high temperatures. In addition, its silicon dioxide (SiO_2) has many properties ideally suited to IC (integrated circuits) manufacturing.

Gallium arsenide is classified as a semiconducting compound. Some of its properties, such as faster operating frequencies (two to three times faster than silicon), low heat dissipation, resistance to radiation, and minimal leakage between adjacent components, makes GaAs an important semiconductor for use in high-performance applications. [77].

The modern age of crystal electronics is based upon materials which are neither metals nor insulators. Such materials are called semiconductors, and their electrical properties are intermediate between those of metals and insulators. This is because of a rather special arrangement of the energy levels of electrons in semiconductors [78].

There are several ways of defining a semiconductor. Historically, the term semiconductor has been used to denote materials with a much higher conductivity than insulators, but a much lower conductivity than metals measured at room temperature. Today there are two more types of conductors: superconductors and semimetals. Typical conductivities of superconductors, metals, semimetals, semiconductors and insulators are listed in Table 3.1. While metals (except for superconductors) and semimetals retain their metallic conductivity even at low temperatures, semiconductors are transformed into insulators at very low temperatures. ln this sense semiconductors and insulators are actually one class of materials, which differs from metals and semimetals, which form another class. This classification is directly connected to the existence of a gap between occupied and empty states, i.e., an energy gap, in semiconductors and insulators. In Table 3.2 the classification according to the energy gap (E_g) is summarized.

Table 3.1 Typical conductivities (σ=l/RA, where l denotes the length, R the resistance, and A the cross sectional area of the conductor) of superconductors, metals, semimetals, semiconductors, and insulators at room temperature.

Type of solid	$\sigma(\Omega^{-1}\,cm^{-1})$	Example
Superconductor (low temperature)	$> 10^{10}$	Pb, $YBa_2Cu_3O_7$
Metal	$10^5 - 10^{10}$	Au, Cu, Pb, Ag
Semimetal	$10^2 - 10^5$	graphite (C), HgTe
Semiconductor	$10^{-9} - 10^2$	Si, Ge, GaAs, InSb, Zn, Se
Insulator	$< 10^{-9}$	quartz (SiO_2), CaF_2

Table 3.2 Classification of solids according to their energy gap (E_g) and carrier density n at room temperature.

Type of solid	E_g (eV)	n (cm^{-3})
Metal	no energy gap	10^{22}
Semimetal	$E_g \leq 0$	$10^{17} - 10^{22}$
Semiconductor	$0 < E_g < 4$	$< 10^{17}$
Insulator	$E_g \geq 0$	$<< 1$

The border line between semiconductors and insulators is rather arbitrary. In particular, the value of the energy gap separating the semiconducting materials from the insulating ones is not well-defined. For example, diamond (C) was considered tor a long time an insulator, but today it is possible to prepare it in such a way that it has semiconducting properties even at room temperature. The important distinction between these two systems originates historically from their different conductivities at room temperature. However, an insulator at room temperature can become a semiconductor at higher temperatures. Therefore, wide energy gap materials are currently under investigation for high temperature electronics.

Another possibility of defining a semiconductor, which is related to the energy gap, is through the free carrier concentration at room temperature. Metals and semimetals have a rather large carrier density; semiconductors exhibit a moderate

carrier density at room temperature, while insulators have a negligible carrier density. Typical carrier densities for these different types of solids are compiled in Table 3.2. The listed densities are intrinsic values, i.e., for pure materials. However, real semiconductors always contain some impurities, which can act as dopants leading to larger values for the carrier densities than the intrinsic ones.

Due to the existence of the energy gap, semiconductors are transparent for energies below the gap, i.e., in the far- to near-infrared region depending on the value of the energy gap. However, they strongly absorb light for energies above the energy gap, typically in the near-infrared to visible regime. This behavior again is in strong contrast to metals, which are usually opaque from the far-infrared to the visible regime. In the absorptive region, the conductivity of semiconductors increases, when they are irradiated [71].

A semiconductor is determined by its chemical composition and atomic structure, which give it technically interesting, tunable electronic properties. A semiconductor is a solid with an electrical conductivity between that of a metal and an insulator. This conductivity is caused by electronic particles, such as electrons, holes, and polarans which are set free by ionization. Such ionization can be produced thermally by light, other particles, or an electric field [79].

Elementary semiconductors are semiconductors where each atom is of the same type such as Ge, Si. These atoms are bound together by covalent bonds, so that each atom shares an electron with its nearest neighbor, forming strong bonds [80]. These are elementary semiconductors such as Si, Ge, and gray tin (α-Sn), which all belong to group IV in the periodic table. Therefore, these systems are usually referred to as group IV semiconductors as shown in Fig. 3.4. Another group IV element is carbon, which solidifies into two structures, diamond and graphite. Diamond is an insulator and has the same crystal structure as Si, Ge, and α-Sn. Graphite is a semimetal and exhibits a hexagonal structure. Sn also exists in two phases, white tin (β-Sn), which is metallic, and semiconducting α-Sn. The last element of the group IV is lead, which is metallic.

II	III	IV	V	VI
	Al	Si	P	S
Zn	Ga	Ge	As	Se
Cd	In	Sn	Sb	Te
Hg				

Figure 3.4 Elements found in elemental and compound semiconductors. Group IV are elemental semiconductors. Compound semiconductors can be formed by combining Groups III and V or II and VI or III and VI.

Group IV elements are exceptional in the periodic table in the sense that the outer shell of the individual atoms is exactly half filled. By sharing one of the four electrons of the outer shell with another Si atom, a three-dimensional crystal structure with no preferential direction (except for graphite) can be realized.

Compound semiconductors are made of two or more elements. Elements from group III (II) can be combined with group V (VI) elements. Group I elements in conjunction with group VII elements lead to wide energy gap insulators, since these materials are formed by ionics bonds and not covalent bonds as III-V and most II-VI semiconductors. Most of the III-V semiconductors exist in the so-called zincblende structure, which is a cubic lattice. Some exist in the wurtzite structure, which corresponds to a hexagonal lattice. GaAs is the best-known III-V compound semiconductor, while GaN, although known for a long time, has only recently become very important stimulating a lot of research on this material [71]. Common examples are CdS or ZnS. These compound semiconductors belong to the II-VI semiconductors so called because first and second elements can be found in group II and group VI of the periodic table respectively. In compound semiconductors, the difference in electro-negativity leads to a combination of covalent and ionic bonding. [80].

Variations of compound semiconductors

Elemental   Si, Ge

II-VI compound   CdS, CdSe, CdTe, ZnS, ZnSe, ZnTe

III-V compound   GaP, GaAs, GaSb, InP, InAs, InSb

IV-VI compound   PbS, PbSe, PbTe

IV-IV compound   SiC

V-VI compound Bi_2Te_3

III-VI compound   AlN, GaN, InN, AlP, AlAs, InSe, InS

Compound semiconductor materials can be predicted by a simple rule. When the total numbers of valence electrons of constituent elements are divided by the number of elements comprising the compound and when this ratio gives four, the compound has a tendency to be semiconducting.
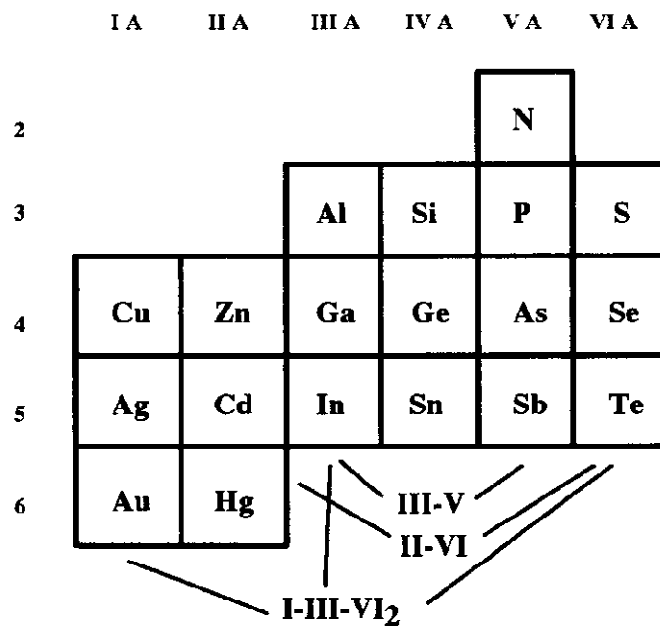
Figure 3.5 Periodic tables for compound semiconductors.

Materials which show semiconducting properties have to obey the following laws.

(i) In the case of elemental semiconductors, the constituent atom has eight electrons including electrons which form covalent bonds and these electrons produce s, p orbital closed shells.

(ii) For compound semiconductors, the condition (i) is applied to each constituent atom.

Elements from IV group to VII group satisfy the first condition (i) and following the second condition (ii), compound semiconductors include these elements.

3.1.4 Band Gap of Semiconductors

The simple energy diagram for a semiconductor at low temperature is shown in Fig. 3.6. At very low temperature the valence bands is full, and the conduction band is empty. Recall that a full band cannot conduct and neither can an empty band. At low temperatures, therefore, semiconductors do not conduct, they behave like insulators.
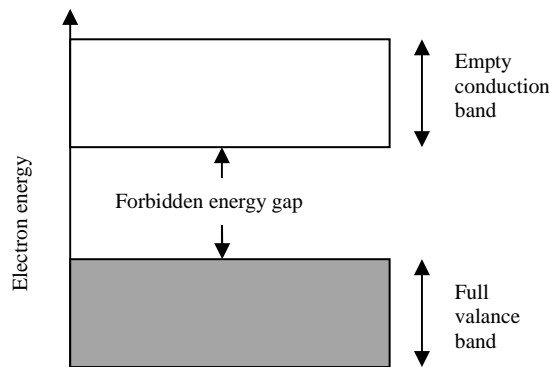
Figure 3.6 Semiconductor energy bands at low temperature.

If energy is supplied to take an electron from the valance bad, across the forbidden energy gap, up into the conduction band, then the electron that has made it to the conduction band is now available for conduction. In addition there is now a vacant electron energy state left in the valance band. This vacant state is called a hole and it behaves like a positive charge carrier with the same magnitude of charge as the electron, but of opposite sign. The band diagram for this situation is shown Fig. 3.7, where the conduction band is populated by electrons leaving a similar number of vacant state (holes) in the valence band. This is an important property of intrinsic, or undoped, semiconductors. The number of electrons in the conduction band must equal the number of holes in the valence band because each electron has given rise to one hole. For extrinsic, or doped, semiconductors where it can be put an excess of either electrons or holes into the material, this is longer true. The hole in the conduction band, except that the hole has positive charge. The hole is not a free

particle, it can only exist within a solid where there is an electron state, some say a missing electron.
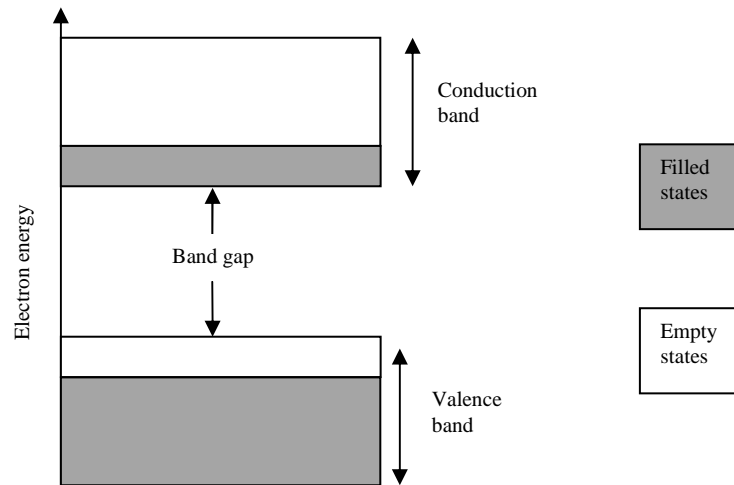
Figure 3.7 Semiconductor energy bands at room-temperature.

Consider Fig. 3.8, which shows just the valence band of a semiconductor in more detail. The semiconductor is at a finite temperature so that some electrons have been thermally excited to the conduction band leaving behind empty states, holes, at the top of the valence band. Since the valence band is now no longer full, it may conduct electric current, and this is just what the hole do.
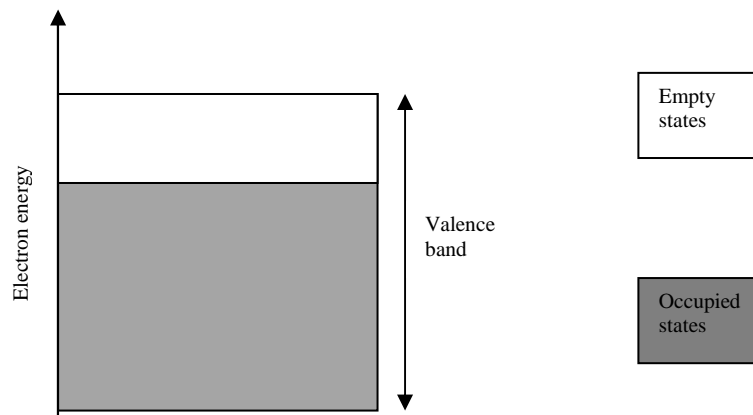
Figure 3.8 Valence band of a semiconductor.

3.2 The Types of Semiconductors

Semiconductors can be also divided into two groups according to their purity: intrinsic and extrinsic semiconductor. Electrical properties can also be changed by doping (adding impurities to the semiconductor material).

3.2.1 Intrinsic Semiconductors

Intrinsic conduction is defined as a semiconduction process that results from the band structure of a pure element or compound. In contrast, extrinsic conduction is a semiconduction process that is facilitated by the presence of impurities, and therefore involves elements or compounds that have already been "doped" with impurity atoms. A semiconductor that is pure is therefore referred to as an intrinsic semiconductor.

The electrical conduction activation energy E depends on the energy needed to break a chemical bond, and may be linked to the standard heat of formation of the crystal from its atoms. It may vary from about 0 to 10 eV. As the thermal activation energy kT increases, a statistically larger fraction of the valency electrons is released and can move under the influence of an electric field. Simultaneously, the empty places they leave behind them can also move. These are called holes, and the same thing happens as if they were particles bearing an equal and opposite charge to that of the electron. This applies to a pure crystal without defects, in which charge carriers consist in equal numbers of electrons and holes. This is an intrinsic semiconductor [81].

In an intrinsic semiconductor, the charge carriers are solely the holes and electrons created in pairs by thermal energy. Electrons in the valence band gain thermal energy and are promoted into the conduction band as temperature increases, leaving behind corresponding holes in the valence band.

Each electron generated in this manner therefore results in an electron-hole pair, i.e., an electron in the conduction band and a hole in the valence band. As such, there is a one-to-one correspondence between the electrons in the conduction band and the holes in the valence band in an intrinsic semiconductor [82]. This is why in an intrinsic semiconductor, $n = p$, where n and p are the intrinsic concentrations of the electrons and holes, respectively.

The general symbol for conductivity of an intrinsic semiconductor is σ. The plot of $\ln\sigma$ versus $1/T$ is a straight line whose slope is $-E_g/2k$, which means that the band gap of an intrinsic semiconductor may be determined experimentally by observing how its conductivity varies with temperature.

The mobility of both electrons and holes decreases linearly with an increase in temperature, but the number of mobile charge carriers increases exponentially with an increase in temperature. With increasing temperature, the exponential increase in the number of carriers is a more dominating factor than the linear decrease in carrier mobility, so the conductivity of an intrinsic semiconductor always increases as temperature increases.

Intrinsic semiconductors or semiconductors that contain no impurities, exhibit conductivities that increases with temperature in a very predictable manner. More specifically, the plot of ln o of an intrinsic semiconductor versus l/T is a straight line whose slope is $-E_g/2k$.

The addition of impurity atoms to intrinsic semiconductors turns them into "doped" or extrinsic semiconductors, which exhibit conductivities that behave differently with temperature variation [83]. Furthermore, the conductivity behavior of an extrinsic semiconductor depends on the type of impurity atoms that it has been doped with.

3.2.2 Extrinsic Semiconductors

Extrinsic semiconductors or semiconductors that have been doped with impurity atoms, exhibit conductivities that behave differently from intrinsic or pure semiconductors. Recall that in an intrinsic semiconductor, the plot of $\ln\sigma$ versus $1/T$ is a straight line whose slope is $-E_g/2k$.

Recall as well that in a solid, energy bands develop to comply with Pauli's Exclusion Principle, such that the electrons in the solid's atoms can only occupy discrete energy levels within the permissible energy bands. If an impurity atom is introduced into a solid, however, its electrons will not be restricted to the energy levels allowed for the host atoms. The electrons of the impurity atom can, in fact, reside in energy levels forbidden to the electrons of the host atoms.

In effect, adding impurity atoms to an intrinsic semiconductor to form an extrinsic semiconductor basically creates new energy levels within the band gap of the semiconductor [84]. Depending on the type of impurities added, these new energy levels in the band gap can be occupied by extra electrons or extra holes from the impurity atoms.

For instance, recall that adding a donor impurity atom (Group V atom) to Si or Ge would result in an "extra" electron that's just loosely bonded to the donor atom. This "donated" electron will reside on an energy level within the upper half of the forbidden band of Si. This energy level occupied by the donated electron is referred to as a "donor level"(E_d).

Adding an Group V atom (such as a P atom) to a silicon or germanium crystal would cause four of its five valence electrons to form covalent bonds with neighboring silicon atoms, while the fifth one would become an "extra" electron that's just loosely bonded to the P atom. For Si and Ge, Group V elements such as P, As, and Sb are therefore known as "donor" impurities, since they "donate" electrons to form materials with excess negative charge. Such materials are referred to as n-type materials.

Similarly, adding a Group III atom (such as a B atom) to a silicon or germanium crystal would cause its three valence electrons to form covalent bonds with three of its four neighboring silicon atoms. This leaves the fourth neighboring Si atom of the B atom missing an "electron", which is basically an "extra" hole. For Si and Ge, Group III elements such as B, Al, and Ga are known as "acceptor" impurities, since they create holes that can "accept" electrons from the valence band. Acceptor impurities form materials with excess positive charge, or p-type materials.

3.2.3 Donors and Acceptors

Semiconductors without any other different atoms added, conduction occurred via electrons in the conduction band and holes in the valence band. For intrinsic material the electrons and holes came in equal numbers, since one conduction electron gave rise to one valence band hole, and we had bipolar (two-carrier) conduction, with the total current being carried by equal numbers of electrons and holes (intrinsic conduction).

Hence, for intrinsic semiconductors:

$$n = p = n_i \tag{3.1}$$

where n is concentration of electrons per unit volume, p is concentration of holes per unit volume, n_i is the intrinsic carrier concentration of the semiconductor under consideration.

The intrinsic carrier concentration n_i depends on the semiconductor material and the temperature. For silicon at 300^0K, n_i has a value of 1.4×10^{10} cm^{-3}. Clearly, Eq. 3.1 can also be written as

$$n \cdot p = n_i^2 \qquad (3.2)$$

The importance of this equation is that it is valid for extrinsic as well as intrinsic material.

Each bond contains two electrons
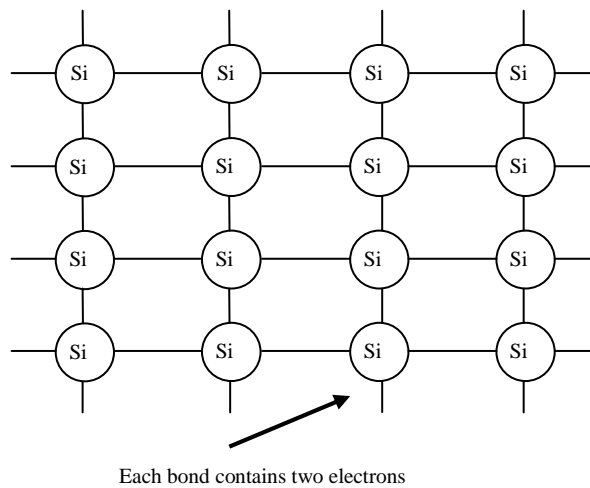
Figure 3.9 Bonding in intrinsic silicon.

The intrinsic silicon case is seen in Fig. 3.9. It's a fiat two-dimensional representation. Silicon, like its neighbors in group IV of the periodic table (carbon and germanium) is a covalently (electron sharing) bonded solid and shows all the characteristic physical properties of covalent solids. It is in a position to see the effect of introducing group III acceptor centre and group V donor centre atoms into the silicon lattice. Fig. 3.10 shows the effect of adding a group III atom (boron in this case) to the silicon lattice. The boron has gone onto a silicon site but it only has three valence electrons, one short for completing the full outer-shell, rare-gas configuration. This deficiency of one electron per impurity atom is in fact the same thing as introducing one hole per impurity atom. This vacant electron state can accept a nearby valence electron (hence the term "acceptor") and in this manner the

vacant electron state appears to move, see Fig. 3.11. There are therefore two ways of introducing holes into semiconductors. One way is to promote an electron from the valence band to the conduction band (by thermal or electromagnetic energy), which leaves a hole in the valence band. This process produces equal numbers of electrons and holes. The other way is to introduce electron deficient (with regard to the silicon bonding requirements) atoms into the silicon lattice. Adding these acceptors to the silicon lattice also introduces holes into the valence band. Very little energy is required to move a nearby valence electron into the vacant state. It is represented this situation as shown in the energy diagram of Fig. 3.12. Here the vacant state (acceptor level) lies just above the valence band, therefore just a little energy can move a valence electron into the vacant state, as required. However, having lost the electron from the valence band to the acceptor level we are now left with a hole in the valence band which is available for conduction. The acceptor level is so close to the valence band edge that very little energy is required to produce the holes; it's very much less than the band-gap energy. Acceptors that introduce energy-levels nearer to the middle of the band gap are called deep acceptors, or deep levels. This partial occupancy of the deep-level acceptors means that not every acceptor gives rise to a conduction hole in the valence band.
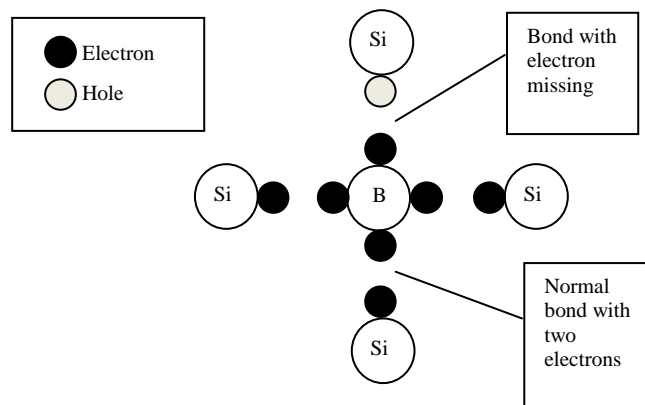
Figure 3.10 Boron bonding in silicon.

It only remains to look at the case of adding electrons to semiconductors without adding additional holes to make n-type material.

External electric field

Simplified Picture

$T_3 > T_2 > T_3$ (Time increasing)

External electric field

Lattice picture
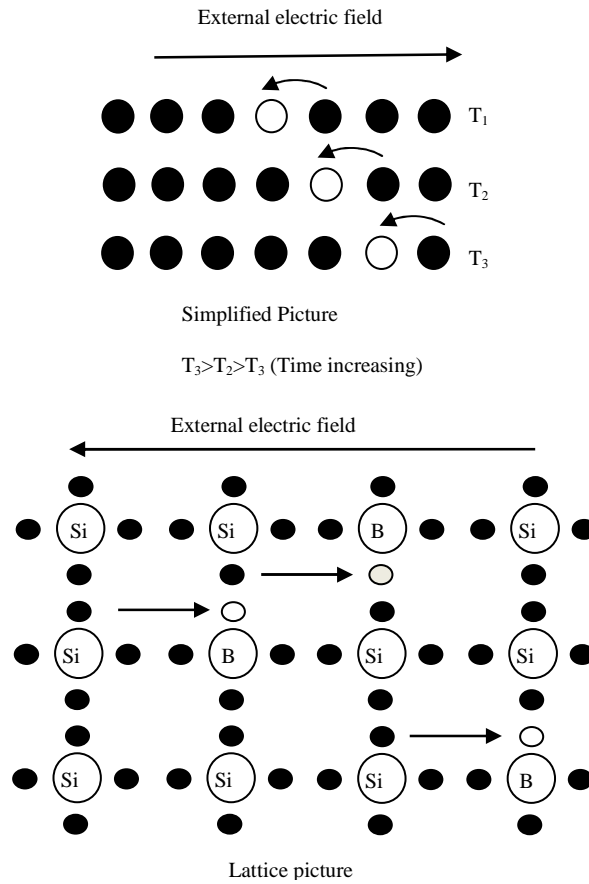
Figure 3.11 Hole movement due to an electric field.

Fig. 3.13 shows the bonding configuration that results when a group V impurity atom is added to the silicon lattice and sits on a lattice site. It is mentioning the impurity atom sitting on a silicon site because it is possible for impurities to go into silicon without sitting on a silicon site. These interstitial impurities are more difficult to analyze and introduce different energy-levels into the semiconductor's band gap. From Fig. 3.10. it can be seen in this figure, one electron too many to satisfy the covalent bonding requirements and this extra electron is in fact very weakly bound to the impurity, which is phosphorus in this case. In a manner exactly analogous to the p-type case it can be shown a suitable energy-level diagram, as seen in Fig. 3.14. Here the impurity atoms form a level just below the conduction band edge; an electron therefore needs very little energy to move from the impurity centre up into the conduction band where it is available for conduction. The impurity centre is said to donate an electron to the conduction band and these are called donor centers. Note that the loss of an electron from the donor centre does not leave a hole at the donor. The donor, together with its neighboring silicon atoms has its full complement of electrons without the extra electron. The extra electron was surplus to

32

bonding requirements; it has been readily given up to the conduction band and is now available for conduction.

Adding donors or acceptors clearly adds a number of electrons (or holes) in proportion to the number of centers added and so the extrinsic (or doped) silicon can be made quite conducting and, therefore, more useful for incorporation in electronic devices.
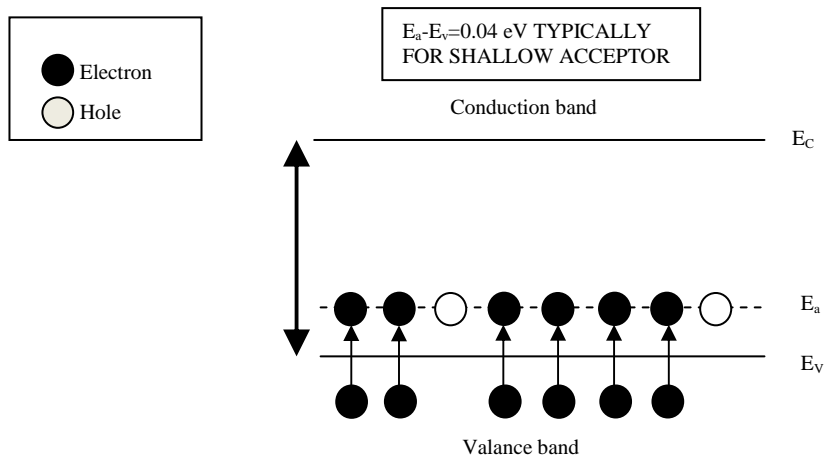
Figure 3.12 Shallow acceptor in silicon.
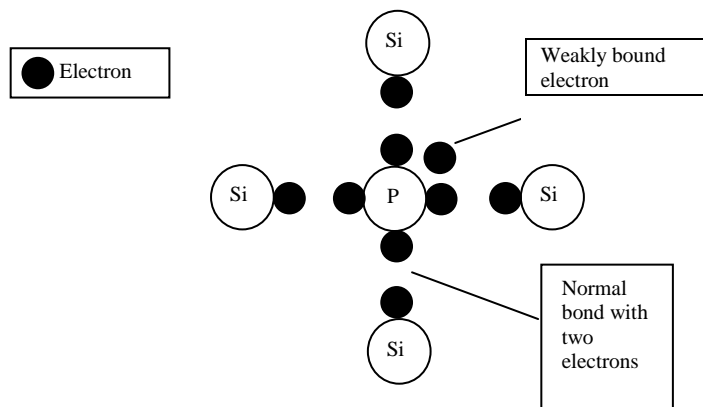
Figure 3.13 Phosphorus bonding in silicon.

1- The donors (and acceptors) have introduced allowed energy-levels in the forbidden energy-gap. The energy gap is forbidden only for pure material, i.e. intrinsic silicon. Once impurity atoms are added to the silicon the perfect crystal lattice is disrupted by these additions (the potential energies change) and it is no

longer forbidden to have allowed states (energy-levels) in the once forbidden energy gap.

2- P-type or n-type silicon is electrically neutral. A neutral atom has gone into neutral silicon. Conduction may be altered by the added, weakly bound electrons or holes, but overall there is charge neutrality. Locally there may not be charge neutrality; when the donor centre loses its electron (becomes ionized) it no longer has its full complement of electrons for charge neutrality. The donor centre when ionized is positively charged. When it has its carrier on it (non-ionized) the donor is neutral [85].
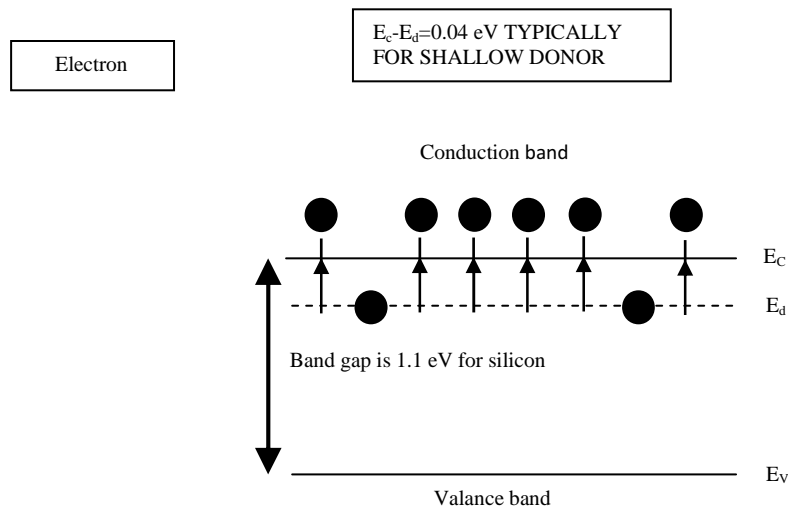
Figure 3.14 Shallow donor in silicon.

3.2.3.1 N-Type Semiconductors

N-type semiconductors are a type of extrinsic semiconductor where the dopant atoms are capable of providing extra conduction electrons to the host material (e.g. phosphorus in silicon). This creates an excess of negative (n-type) electron charge carriers. When a pentavalent (donor) impurity, like arsenic, is added to germanium, it will form covalent bonds with the germanium atoms. Notice the arsenic atom in the center of the lattice. It has five valence electrons in its outer shell but uses only four of them to form covalent bonds with the germanium atoms, leaving one electron relatively free in the crystal structure. Pure germanium may be converted into an n-type semiconductor by "doping" it with any donor impurity having five valence electrons in its outer shell. Since this type of semiconductor (n-

type) has a surplus of electrons, the electrons are considered majority carriers, while the holes, being few in number, are the minority carriers.

The arsenic atoms diffuse uniformly throughout the molten silicon. Most of the atoms in the crystal are still silicon, but occasionally we may find an arsenic atom surrounded by four silicon atoms as shown in Fig. 3.15(a). Each pentavalent arsenic atom forms covalent bonds with four adjacent silicon atoms. Four of the arsenic atom's valence electrons are thus used to form covalent bonds, leaving one extra electron. The extra electron becomes a free electron (conduction electron) because it is not attracted to any atom. The number of these conduction electrons can be controlled by the amount of impurity added to silicon. Since the valence orbit cannot hold more than eight electrons, and the arsenic atom already has them due to sharing of electrons with the four neighboring silicon atoms, one of arsenic atom's original valence electron becomes extra and behaves as a free electron travelling in a conduction band orbit. In effect, the pentavalent or donor atom has produced one free electron. Fig. 3.15(b) shows the energy bands of such a doped crystal. Since each arsenic atom contributes one free electron, the conduction band now has many free electrons; a few thermally produced holes may also be present in the valence band as shown in Fig. 3.15(b).

(a)   (b)
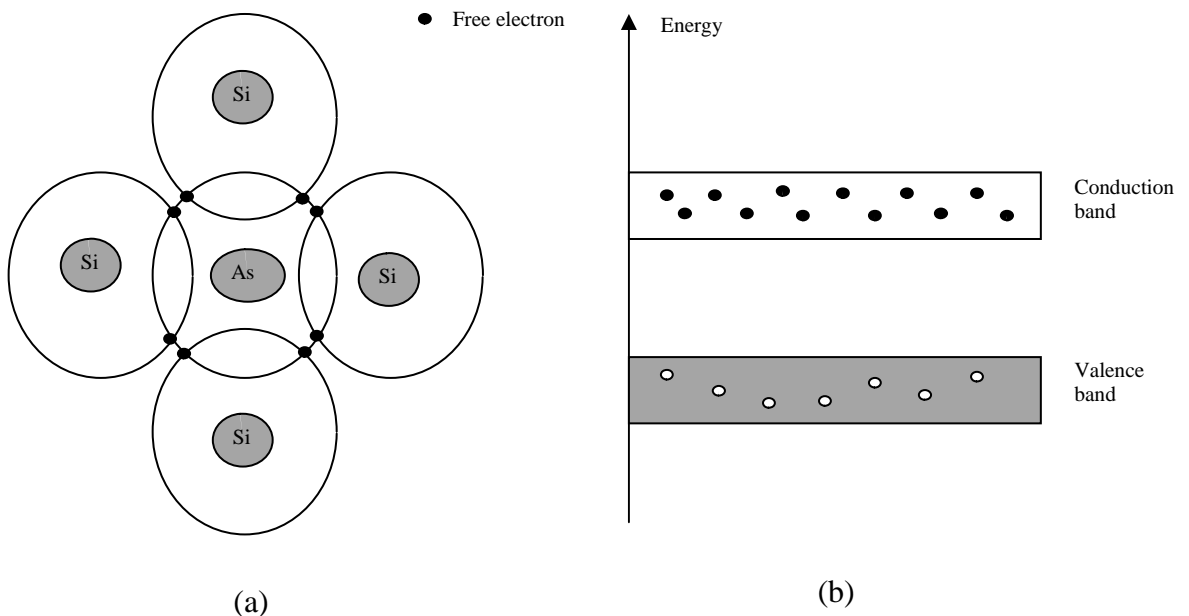
Figure 3.15 Pentavalent doping: (a) an arsenic atom produces a free electron, (b) the conduction band of Si crystal has many free electrons and the valence band has only a few holes.

3.2.3.2 P-Type Semiconductors

The number of holes in a pure silicon crystal can be increased by adding trivalent impurities like boron, aluminum, and gallium. Suppose aluminum has been used to dope pure silicon. After the molten Si has cooled and formed a crystal, we would find that an Al atom is surrounded by four Si atoms as shown in Fig. 3.16(a). Since the Al atom originally had only three valence electrons and each neighbor shares one electron, only seven electrons are in the valence orbit. This means that it is still capable of accepting one electron or in other words, a hole appears in each of the Al atoms valence orbits. A trivalent atom is also known as an acceptor atom because each hole it contributes may accept an electron during recombination.

Fig. 3.16(b) shows the energy bands. A direct result of the trivalent doping is the presence of extra holes in the valence band. There are only a few free electrons in the conduction band owing to the thermally produced electron-hole pairs. This type of doped Si is known as a p-type semiconductor (p for positive). In a p-type semiconductor, the holes are the majority carriers and electrons are the minority carriers [86].

(a)   (b)
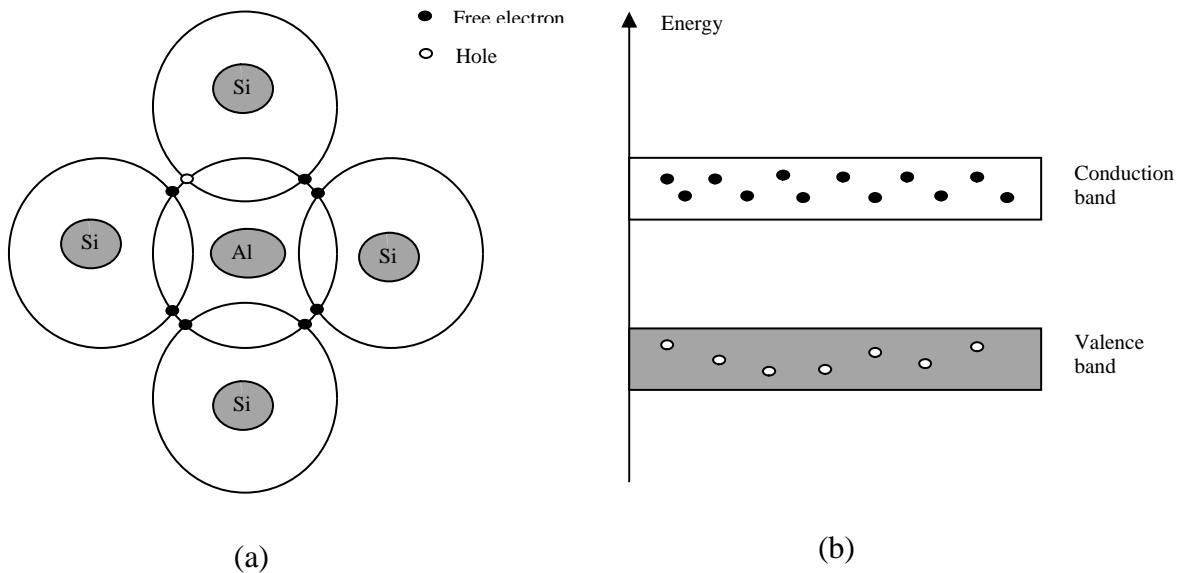
Figure 3.16 Trivalent doping; (a) an aluminum atom produces a hole, (b) the valence band of the Si crystal has many holes and the conduction band has only a few electrons.

3.3 Valence Band and Conduction Band

Chemical reactions originate from the exchange of electrons from the outer electronic shell of atoms. Electrons from the most inner shells do not participate in chemical reactions because of the high electrostatic attraction to the nucleus. Likewise, the bonds between atoms in a crystal, as well as electric transport phenomena, are due to electrons from the outermost shell. In terms of energy bands, the electrons responsible for forming bonds between atoms are found in the last occupied band, where electrons have the highest energy levels for the ground-state atoms. However, there are an infinite number of energy bands. The first (lowest) bands contain core electrons such as the ls electrons which are tightly bound to the atoms. The highest bands contain no electrons. The last ground-state band which contains electrons is called the valence band, because it contains the electrons that form the -often covalent- bonds between atoms.

The permitted energy band directly above the valence band is called the conduction band. In a semiconductor this band is empty of electrons at low temperature ($T=0^0K$). At higher temperatures, some electrons have enough thermal energy to quit their function of forming a bond between atoms and circulate in the crystal. These electrons "jump" from the valence band into the conduction band, where they are free to move. The energy difference between the bottom of the conduction band and the top of the valence band is called "forbidden gap" or "bandgap" and is noted E_g.

In a more general sense, the following situations can occur depending on the location of the atom in the periodic table (Fig. 3.17):

A: The last (valence) energy band is only partially filled with electrons, even at $T=0^0K$.

B: The last (valence) energy band is completely filled with electrons at $T=0^0K$, but the next (empty) energy band overlaps with it (i.e.: an empty energy band shares a range of common energy values; $E_g<0$).

C: The last (valence) energy band is completely filled with electrons and no empty band overlaps with it ($E_g>0$).

In cases 'a' and 'b', electrons with the highest energies can easily acquire an infinitesimal amount of energy and jump to a slightly higher permitted energy level, and move through the crystal. In other words, electrons can leave the atom and move in the crystal without receiving any energy. A material with such a property is a metal. In case 'c', a significant amount of energy (equal to E_g or higher) has to be transferred to an electron in order for it to "jump" from the valence band into a permitted energy level of the conduction band. This means that an electron must receive a significant amount of energy before leaving an atom and moving "freely" in the crystal. A material with such properties is either an insulator or a semiconductor.
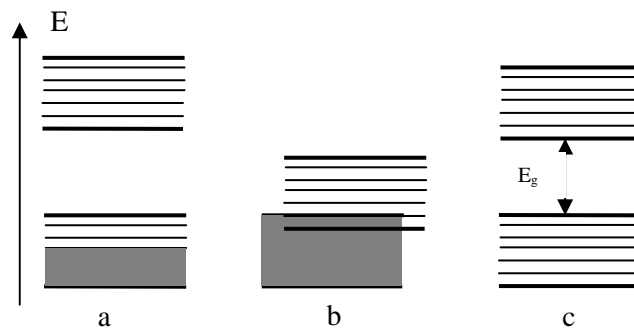
Figure 3.17 Valence band (bottom) and conduction band in a metal (a and b) and in a semiconductor or an insulator(c).

The distinction between an insulator and a semiconductor is purely quantitative and is based on the value of the energy gap. In a semiconductor E_g is typically smaller than 2 eV and room-temperature thermal energy or excitation from visible-light photons can give electrons enough energy for "jumping" from the valence into the conduction band. The energy gaps of the most common semiconductors are: 1.12 eV (silicon), 0.67 eV (germanium), and 1.42 eV (gallium arsenide). Insulators have significantly wider energy bandgaps: 9.0 eV (SiO_2), 5.47 eV (diamond), and 5.0 eV (Si_3N_4). In these materials room-temperature thermal energy is not large enough to place electrons in the conduction band.

Beside elemental semiconductors such as silicon and germanium, compound semiconductors can be synthesized by combining elements from column IV of the periodic table (SiC and SiGe) or by combining elements from columns III and V (GaAs, GaN, InP, AlGaAs, AlSb, GaP, AlP and AlAs). Elements from other columns

can sometimes be used as well (HgCdTe, CdS,...). Diamond exhibits semiconducting properties at high temperature, and tin (right below germanium in column IV of the periodic table) becomes a semiconductor at low temperatures. About 98% of all semiconductor devices are fabricated from single-crystal silicon, such as integrated circuits, microprocessors and memory chips. The remaining 2% make use of III-V compounds, such as light-emitting diodes, laser diodes and some microwave-frequency components.

III	IV	V
B	C	N
Al	Si	P
Ga	Ge	As
In		Sb

Figure 3.18 Main elements used in semiconductor technology (elemental semiconductors such as Si, and compound semiconductors such as GaAs).

It is worthwhile mentioning that it is possible for non-crystalline materials to exhibit semiconducting properties. Some materials, such as amorphous silicon, where the distance between atoms varies in a random fashion, can behave as semiconductors. The mechanisms for the transport of electric charges in these materials are, however, quite different from those in crystalline semiconductors.

It is convenient to represent energy bands in real space instead of k-space. By doing so one obtains a diagram such as that of Fig. 3.19, where the x-axis defines a physical distance in the crystal. The maximum energy of the valence band is noted E_V, the minimum energy of the conduction band is noted E_C, and the width of the energy bandgap is E_g. It is also appropriate to introduce the concept of a Fermi level. The Fermi level, E_F, represents the maximum energy of an electron in the material at zero degree Kelvin (0^0K). At that temperature, all the allowed energy levels below the Fermi level are occupied, and all the energy levels above it are empty. Alternatively, the Fermi level is defined as an energy level that has a 50% probability of being filled with electrons, even though it may reside in the bandgap. In an insulator or a semiconductor, we know that the valence band is full of electrons, and the conduction band is empty at 0^0K. Therefore, the Fermi level lies somewhere in

the bandgap, between E_V and E_C. In a metal, the Fermi level lies within an energy band [87].
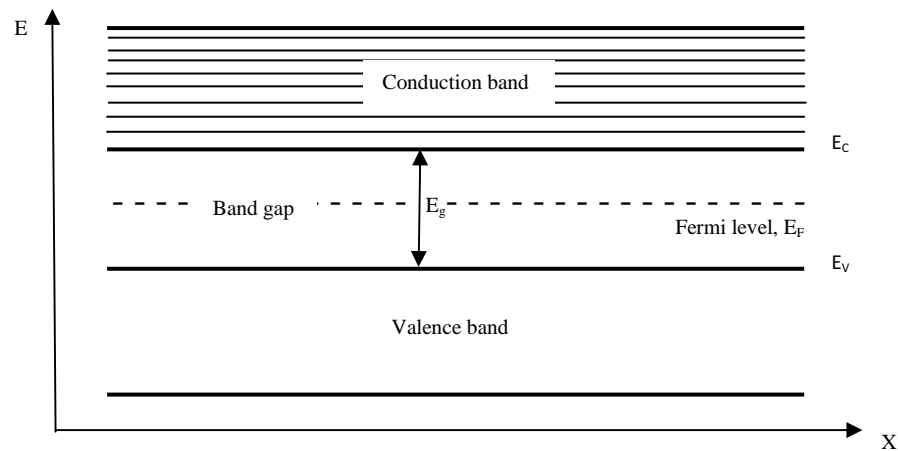
Figure 3.19 Valence and conduction band in real space.

3.4 Direct and Indirect Gap Transitions

In semiconductor physics, a direct bandgap means that the minimum of the conduction band lies directly above the maximum of the valence band in momentum space. In a direct bandgap semiconductor, electrons at the conduction band minimum can combine directly with holes at the valence band maximum, while conserving momentum. The energy of the recombination across the bandgap will be emitted in the form of a photon of light. This is radiative recombination, also called spontaneous emission. In indirect bandgap semiconductors such as crystalline silicon, the momentum of the conduction band minimum and valence band maximum are not the same, so a direct transition across the bandgap does not conserve momentum and is forbidden. Recombination occurs with the mediation of a third body, such as a phonon or a crystallographic defect, which allows for conservation of momentum. These recombination will often release the bandgap energy as phonons, instead of photons, and thus do not emit light. As such, light emission from indirect semiconductors is very inefficient and weak [88].
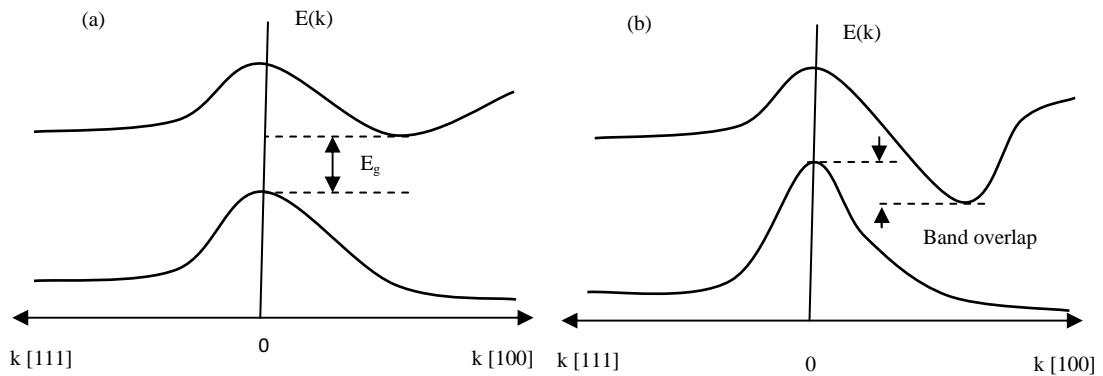
Figure 3.20 Examples of energy band extreme (minimum of the conduction band and maximum of the valence band in two crystals). In crystal (a), E_g is the bandgap energy. There is no bandgap in crystal (b) because the conduction and the valence bands overlap.

It is impossible to represent the energy bands as a function of $k = k (k_x, k_y, k_z)$ for a three-dimensional crystal in a drawing made on a two-dimensional sheet of paper. One can, however, represent $E(k)$ along main crystal directions in k-space and place them on a single graph. For example, Fig. 3.20 represents the maximum of the valence band and the minimum of the conduction band as function of k in the [100] and the [111] directions for two crystals. Crystal (a) is an insulator or a semiconductor ($E_g>0$); crystal (b) is a metal ($E_g<0$).

The energy band diagrams, plotted along the main crystal directions, allow us to analyze some properties of semiconductors. For instance, in Fig. 3.21.(b) the minimum energy in the conduction band and the maximum energy in the valence band occur at the same k-values (k=0). A semiconductor exhibiting this property is called a direct-band semiconductor. Examples of direct-bandgap semiconductors include most compound elements such as gallium arsenide (GaAs). In such a semiconductor, an electron can "fall" from the conduction band into the valence band without violating the conservation of momentum law, i.e. an electron can fall from the conduction band to the valence band without a change in momentum. This process has a high probability of occurrence and the energy lost in that "jump" can be emitted in the form of a photon with an energy $hv=E_g$. In Fig. 3.21.(a), the minimum energy in the conduction band and the maximum energy in the valence band occur at different k-values. A semiconductor exhibiting this property is called an indirect bandgap semiconductor. Silicon and germanium are indirect-bandgap

41

semiconductors. In such a semiconductor, an electron cannot "fall" from the conduction band into the valence band without a change in momentum. This tremendously reduces the probability of a direct "fall" of an electron from the conduction band into the valence band [87].
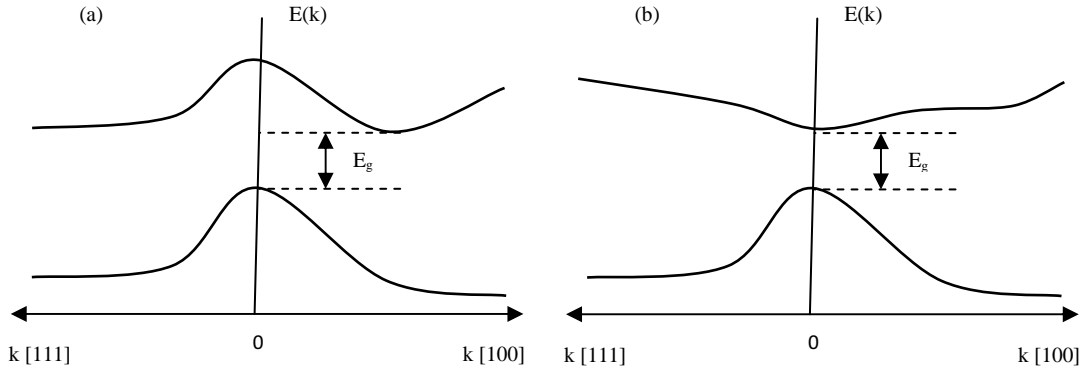
Figure 3.21(a):Indirect bandgap semiconductor, (b):Direct bandgap semiconductor.

3.5 Fundamentals of Absorption

The fundamental absorption refers to band-to-band or to exciton transitions, i.e., to the excitation of an electron from the valence band to the conduction band. The fundamental absorption, which manifests itself by a rapid rise in absorption, can be used to determine the energy gap of the semiconductor.

The absorption coefficient $\alpha(h\nu)$ for a given photon energy $h\nu$ is proportional to the probability P_{if} for the transition from the initial state to the final state and to the density of electrons in the initial state, n_i, and also to the density of available (empty) final states, n_f, and this process must be summed for all possible transitions between states separated by an energy difference equal to $h\nu$:

$$P_{if} n_i n_f \tag{3.3}$$

3.5.1 Allowed Direct Transitions

It is considered between two direct valleys where all the momentum conserving transitions are allowed Fig. 3.22, i.e., the transition probability is independent of photon energy.
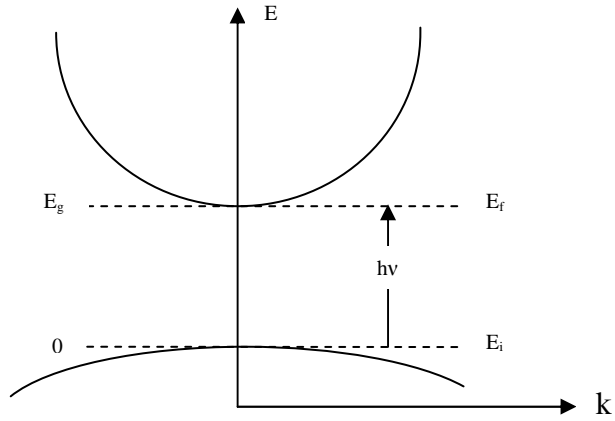
Figure 3.22 Two direct valleys where all the momentum conserving transitions are allowed.

Every initial state at E_i is associated with a final state at E_f such that

$$E_f = hv - |E_i| \tag{3.4}$$

But in parabolic bands,

$$E_f - E_g = \frac{h^2 k^2}{8\pi^2 m_e^*} \tag{3.5}$$

and

$$E_i = \frac{h^2 k^2}{8\pi^2 m_h^*} \tag{3.6}$$

Therefore,

$$hv - E_g = \frac{h^2 k^2}{8\pi^2} \left(\frac{1}{m_e^*} + \frac{1}{m_h^*} \right) \tag{3.7}$$

Since, in general, the valleys are rotational ellipsoids instead of spherical surfaces, the effective mass is not isotropic; then an average density of state effective mass is used:

$$m^* = (m_l^* m_{t1}^* m_{t2}^*)^{1/3} \tag{3.8}$$

where m_l^* is the longitudinal effective mass and m_{t1}^* and m_{t2}^* are the two transverse masses. Hence the absorption coefficient which is the function of hv, α is

$$\alpha(hv) = A^* \left(hv - E_g \right)^{1/2} \tag{3.9}$$

where A^* is given by:

43

$$A^* = \frac{q^2 \left(2\frac{m_h^* m_e^*}{m_h^* + m_e^*}\right)^{3/2}}{nch^2 m_e^*} \tag{3.10}$$

3.5.2 Forbidden Direct Transitions

In some materials, quantum selection rules forbid direct transitions at model of Fig. 3.23 this means that the transition probability increases proportionately to $\left(hv - E_g\right)^{1/2}$, the absorption coefficient has the following spectral dependence:

$$\alpha(hv) = A\left(hv - E_g\right)^{1/2} \tag{3.11}$$

where A is given by

$$A^* = \frac{4}{3}\frac{q^2 \left(\frac{m_h^* m_e^*}{m_h^* + m_e^*}\right)^{5/2}}{nch^2 m_e^* m_h^* hv} \tag{3.12}$$
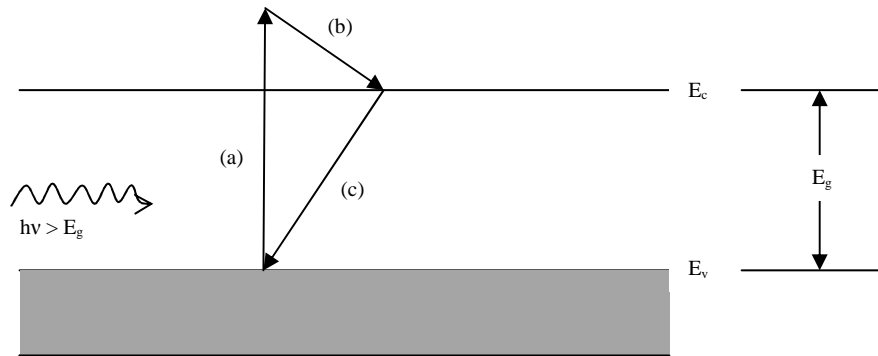
Figure 3.23 Optical absorption of a photon with hv>E_g: (a) an EHP(electron-hole production) is created during photon absorption; (b) the excited electron gives up energy to the lattice by scattering events; (c) the electron recombines with a hole in the valence band.

3.6 Optical Absorption

An important technique for measuring the band gap energy of a semiconductor is the absorption of incident photons by the material. In this process, photons selected wavelengths are directed at the sample and the relative transmission of the various photons is observed. Since photons with energies greater than the band

gap energy are absorbed while photons with energies less than band gap are transmitted, this process gives an accurate measure of the band gap energy.

3.6.1 Absorption Constant and Band Gap

If a beam of photons with $h\nu > E_g$ falls on a semiconductor, there will be some predictable amount of absorption, determined by the properties of the material. It would be expected the ratio of transmitted to incident light intensity to depend on the photon wavelength and the thickness of the sample. To calculate this dependence, it is assumed that a photon beam of intensity I_o (photons/cm^2-sec) is directed at a sample of thickness I (Fig. 3.24).
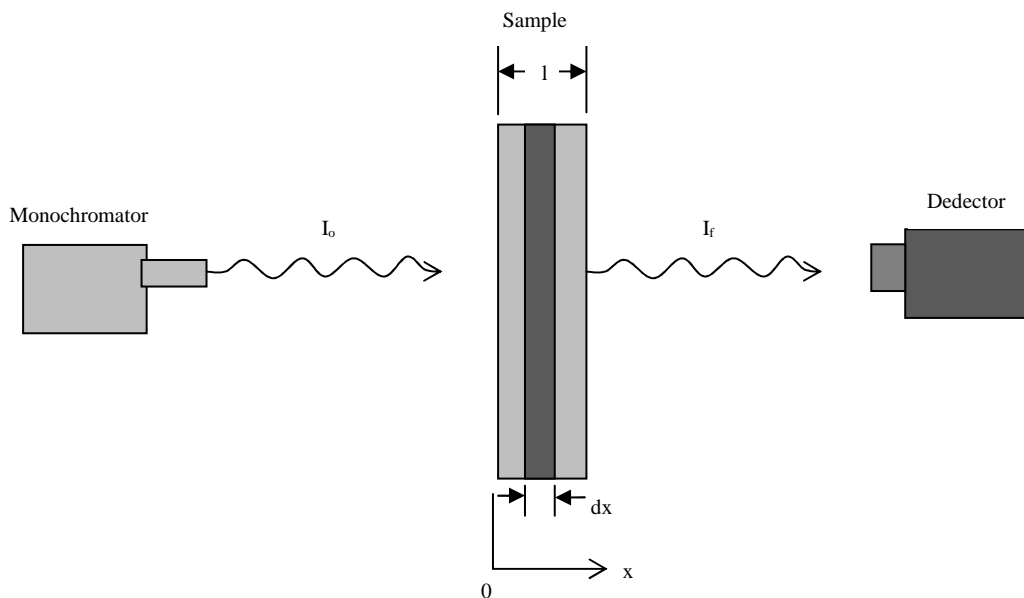
Figure 3.24 Optical absorption experiment.

The beam contains only photons of wavelength λ, selected by a monochromator. As the beam passes through the sample, its intensity at a distance x from the surface can be calculated by considering the probability of absorption within any increment dx. Since a photon which has survived to x without absorption in any dx is constant [89].

Assume that a semiconductor is illuminated from a light source with $h\nu$ greater than E_g and a photon flux of I_o. As the photon flux travels through the semiconductor, the fraction of the photons absorbed is proportional to the intensity of the flux. Therefore the number of photons absorbed within an incremental distance Δx (Fig. 3.25a) is given

(a)

(b)
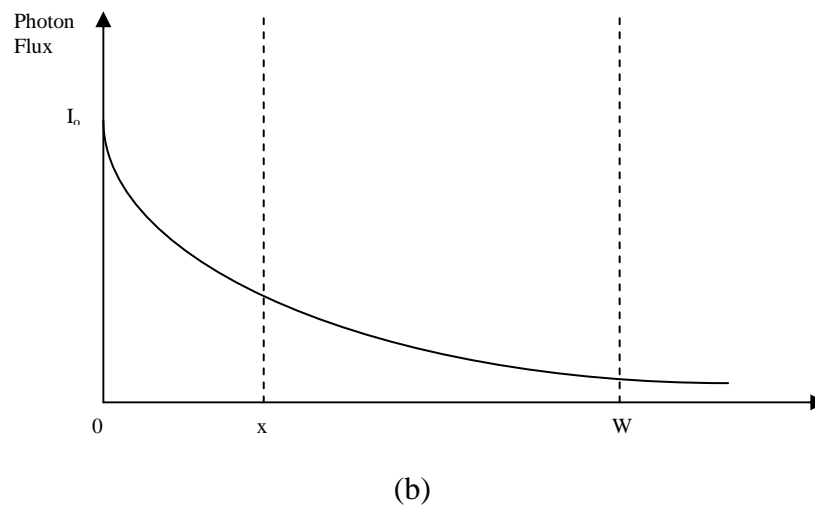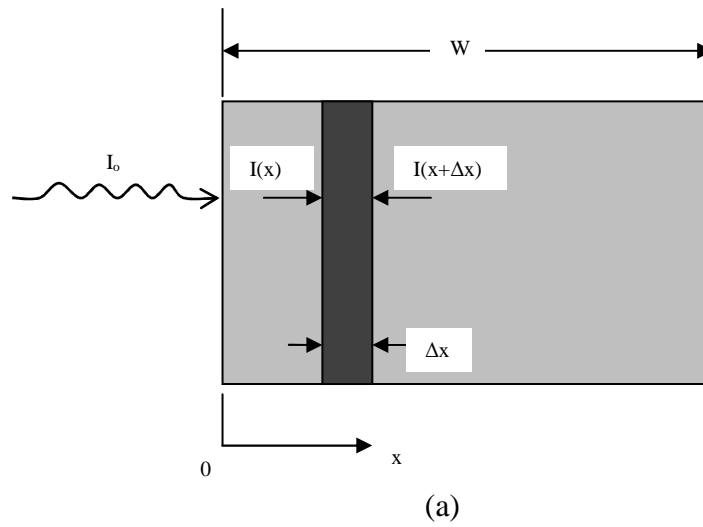
Figure 3.25 Optical absorption (a) Semiconductor under illumination (b) Exponential decay of photon flux.

$\alpha I_o \Delta x$, where is a proportionality constant defined as the absorption coefficient. From continuity of photon flux as shown in Fig.3.25a, we obtain

$$I(x + \Delta x) - I(x) = -aI(x)\Delta x \qquad (3.13)$$

or

$$\frac{dI(x)}{dx} = -aI(x) \qquad (3.14)$$

The negative sign indicates decreasing intensity of the photon flux due to absorption. The solution of Eq. 3.14 with the boundary condition I(0)=I$_0$ at x=0 is

$$I(x) = I_0 e^{-ax} \qquad (3.15)$$

The fraction of photon flux that exists from the other end of the semiconductor at x=I (Fig. 3.25b) is

$$I(I) = I_0 e^{-aI} \qquad (3.16)$$

As an alternative to a transmission experiment, it is possible to monitor the resistance of the sample and observe the photon energy at which absorption takes place. Since absorbed photons create EHP's and these carriers are able to participate in conduction, the conductivity of the sample will increase when photons are absorbed. This change in the conductivity with optical absorption called photoconductivity.

Fig. 3.26 indicates the band gap energies of some of the common semiconductors relative to the visible infrared and ultraviolet portions of the spectrum. It is observed that GaAs, Si, Ge, and InSb lie outside the visible region so that if the eye is to be used as detector in the transmission experiment, an infrared converter tube must be used. Other semiconductors, such as GaP and CdS, have band gaps wide enough to pass photons in the visible range. It is important to note here that a semiconductor absorbs photons with energies equal to the band gap, or larger [89].
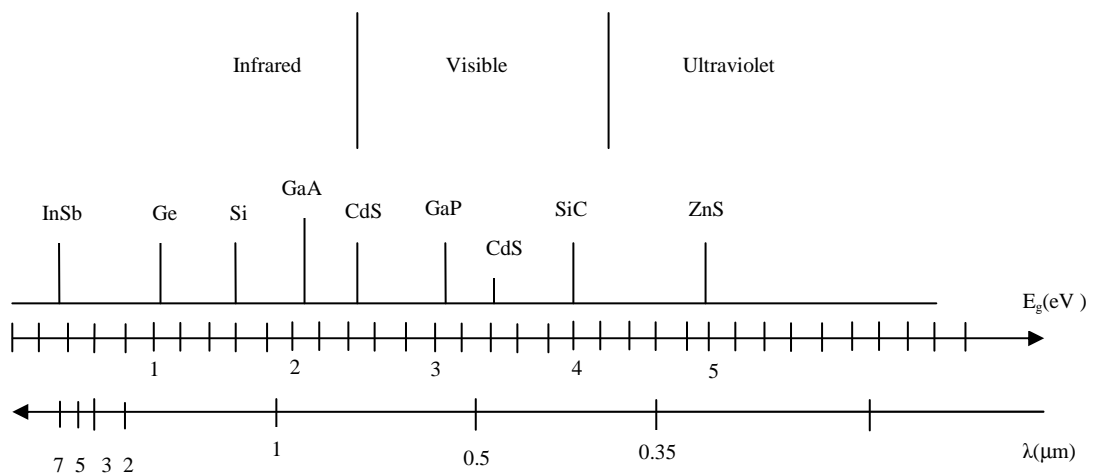
Figure 3.26 Band gaps of some common semiconductors relative to the optical spectrum.

CHAPTER 4
EXPERIMENTAL STUDIES

4.1 Thin Film Production Techniques
4.1.1 Spray Pyrolysis Method

The spray pyrolysis technique (or solution spraying) for the growth of semiconducting films is a method of spraying a suitable solution mixture onto a heated substrate. It is a convenient and economical method for the deposition of such materials. This technique is simply consisting of spraying a finely atomized solution onto a suitable hot substrate.

Spray pyrolysis is a process in which a thin film is deposited by spraying a solution on a heated surface, where the constituents react to form a chemical compound. The chemical reactants are selected such that the products other than the desired compound are volatile at the temperature of deposition. There have been many studies in this area since the pioneering paper by Chamberlin&Skarman on CdS films for solar cells in 1966, among them a review of transparent conductors and a bibliography Pamplin presented at a conference on spray pyrolsis.

Spray pyrolysis is a powerful technique to synthesize a wide variety of high purity, chemically homogenous ceramic powders. Large quantities of oxide powders with homogeneous particle sizes and crystallite sizes less than 100 nanometers may be produced by this method, which is both simple and allows for continuous operation. Due to the small crystallites, the powders offer the opportunity to tailor materials on a nano-scale.

4.1.1.1 Deposition Apparatus

The apparatus used to carry out the chemical spray process consists basically of a device to atomize the spray solution and some sort of substrate heater. A typical experimental setup presented by Chamberlin&Skarman was used. Our setup consists of a reaction chamber of Pyrex glass joined to its lower part with a plate heated by electrical resistance. On the plate is placed the substrate, whose temperature is

measured with a thermocouple, located under the substrate. Above, at an established distance, is fixed a glass spraying nozzle, through which the adequate solution is sprayed (from a receiver) by means of the carrier gas. The gases are exhausted through a hole, situated at the lower part of the chamber.
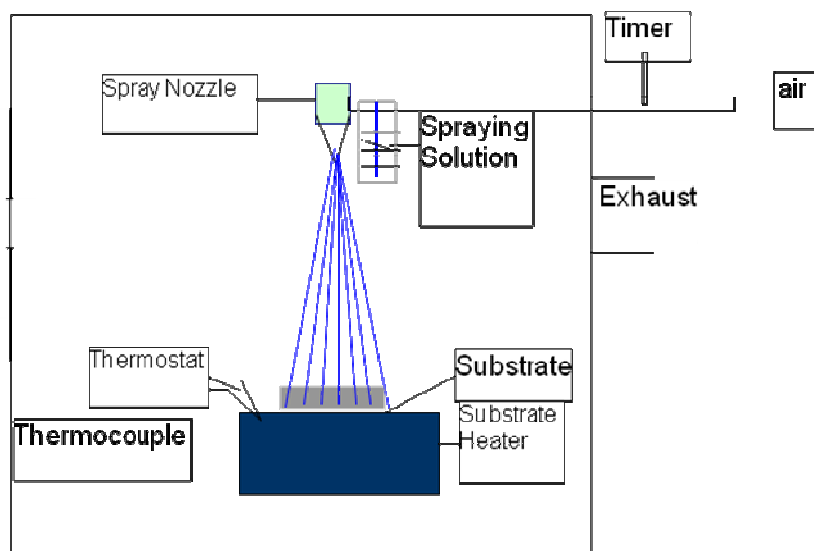
Figure 4.1 Schematic diagram of the spray pyrolysis system.

Spraying system: This is used to produce the bubbles from the spraying solution. In this study, air was be used as carrier gas and the flow rate of the spraying solution was be regulated by air.

Heater: This is used to heat the substrates. It is consisted of a steel plate with a resistance coil lying under it. The power of the heater is 2500 watts and it operates at 220 volts and 50 Hz (AC).

Temperature control system: A thermostat is used to keep the substrates at required temperatures. One of the most important factors which play a vital role for producing high quality thin film samples is to keep the substrates at required temperatures. The substrate temperature is controlled to within an accuracy of $\pm 5^0$C by thermostat system.

4.2 Growth Mechanism of CuS Thin Films by the Spraying Pyrolysis Method

4.2.1 Substrate Preparation

The physical properties of substrates on which thin films is deposited, play a vital role in the growth of good quality thin film samples. The film properties are very strongly dependent on the crystal structure of substrate. The crystalline films can be deposited on a noncrystalline material such as glass, ceramic and mica. For example, a highly crystalline film from the CuS solutions can be developed on an amorphous substrate.

In this study, glass is used as substrate because of its cheepless when compared to other types of substrate. The preparation of glass substrate is as follows. Firstly, the glass substrates are cut into 0.5 cm^2 in size. A cleaning process of the glass substrate is carried out in four steps as seen in following Fig. 4.2.
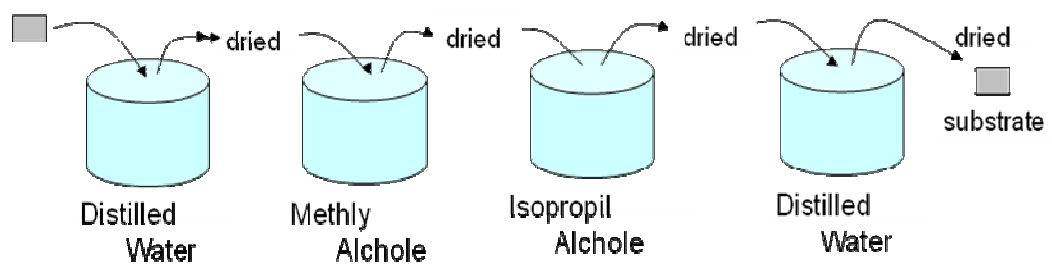
Figure 4.2 The cleaning process of the glass substrate.

4.2.2 Cleaning Process of the Glass Substrate

The cleaning process is as follows:

1. The glass substrate is immersed into the distilled water to clean the dust on its surface for 15 minutes. Then it is taken out from the distilled water and dried.

2. The substrate which is taken from the first cup and dried, is immersed into the methyl alcohol and left there for 15 minutes to clean the oil substance on the surface of the substrate, and then it is taken out from this liquid and dried in air.

3. The dried substrate is immersed into the third cup filled with isopropyl alcohol and it is treated again for 15 minutes to obtain a smooth surface.

4. Finally, the substrate is treated with the distilled water as in the first step to clean all the residues remaining on the surface of substrate during the other processes.

4.2.3 Spraying Solution Preparation

The films of CuS were obtained by spray pyrolysis in air atmosphere. The films were prepared using the aqueous solutions containing copper chloride ($CuCl_2$, Merck, purity 98%) and thiourea ($SC(NH_2)_2$, Merck, purity 98%). The spraying solution is prepared for the production of CuS thin film as follow; firstly, the required amounts of $CuCl_2$ and $SC(NH_2)_2$ salts are weighted by high sensible electronic balance and stirred together into a cup containing the distilled water of 100 cm^3 to form the solution. Different spraying solutions were used for the production of semiconducting CuS thin films with different compositions.

The CuS thin films were prepared by spraying an aqueous solution of $CuCl_2$ and $SC(NH_2)_2$ on the high cleaned glass substrate. The substrate temperature was kept constant at 250, 350 and 450^{0}C using electronic temperature controller with an accuracy of ±5 °C. The atomization of the chemical solution into a spray of fine droplets is effected by the spray nozzle, with the help of compressed air by the air pump as carrier gas. The solution was sprayed through a nozzle onto glass substrates (0.5 cm^2) using air as carrier gas with a pressure of 1.5 bars. Totally, 100 cm^3 of solution was used and sprayed for 45 minutes. The molar ratio of the copper and sulphur sources of Cu:S ; 1:1, 1:2 and 2:1 were used, whereas the concentration of $CuCl_2$ was kept constant at 0.05 M in stock solution and thin films were prepared in the normal atmospheric conditions. During the spraying process the substrates were heated by an electrical heater. The flow rate of the solution was kept at about 5cm^3min^{-1}. During the preparation of deposits, the solution and air flow rates were kept constant at 2 cm^3/min and 45 cm^3/min^{-1}, respectively. Commercial high cleaned glass (0.5 cm^2 in size) was used as substrates for all the deposition. The distance between the nozzle and the substrate was maintained at 35 cm.

4.2.4 Development of CuS Thin Films

To develop polycrystalline CuS thin film samples, a 100 cm^3 spraying solution of copper chloride $CuCI_2$ and thiourea $SC(NH_2)_2$ with different ratios were used. The CuS thin films were prepared by spraying an aqueous solution of $CuCI_2$ and $SC(NH_2)_2$ on glass substrate kept at different temperature. The atomization of the

chemical solution into a spray of fine droplets is effected by the spray nozzle, with the help of compressed air as carrier gas.

During the spraying process the substrates were heated by an electrical heater. The spraying solutions were sprayed onto the glass substrate which was kept at different temperature. When the solution droplets reach to the heated glass substrate surface, the following chemical reaction occurs,

$$CuCl_2 + SC(NH_2)_2 + 2H_2O \longrightarrow CuS + CO_2 + 2NH_4Cl$$
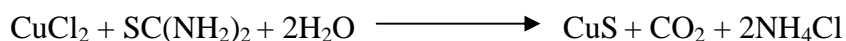
As seen from this reaction, CuS thin film is formed on the glass substrate surface, the other chemicals (CO_2 and NH_4Cl) release as gas and vapor. All spraying processes were carried out in air.

4.3 Measurement Techniques

4.3.1 The Thickness Determination of CuS Thin Films

The thicknesses of the samples were obtained by using the weighing method. This method is explained by the following expression:

$$t = \frac{(m_2 - m_1)}{qA} \tag{4.1}$$

where ρ is the density of the CuS thin films (ρ=4,68 g/cm^3), m_1 is the weight of the glass substrate before the film growth and m_2 is the weight of the same glass substrate after the CuS sample growth on it, and A is the area of the glass substrate.

4.3.2 Optical Studies

An important technique used for the determination of the band gap energy of a semiconductor is the absorption of incident photons by material. Optical absorption studies of the sprayed CuS thin films on the glass substrate have been carried out in the wavelength range of 300 nm to 900nm employing a UV/VIS spectrophotometer (Jasco 7800 model). The absorption coefficient of sample corresponding to different wavelengths can be calculated from following equation:

$$\frac{I}{I_0}(transmission) = e^{-at} \tag{4.2}$$

where t is the thickness of the thin film sample, T=I/I$_0$ is transmittance. (I$_0$ is incident light intensity and I is transmitted light intensity). By using α values, the optical

band gap of the thin film sample can be determined by means of the following equation:

$$\alpha = \frac{A}{h\nu}\left(h\nu - E_g\right)^{1/2}$$

(4.3)

where A is a constant, E_g energy band gap of thin film, h is Planck constant, $\nu = c/\lambda$, c is light speed and λ is wavelength of light. The dependences of $(\alpha h\nu)^2$ as a function of photon energy $h\nu$ indicates the direct nature of band-to-band transitions for the studied samples. The values of optical bandgap, E_g, have been determined by extrapolating the lineer portions of respective curves to $(\alpha h\nu)^2 \to 0$.

4.4 The Crystal Structure of the Thin Film Samples

4.4.1 X-Ray Diffraction Study

Structural properties of the deposited thin films were studied by using X-ray diffraction (XRD) technique. The X-ray measurements were performed using CuK_α radiation ($\lambda = 1.542 \text{Å}$) from a conventional θ-2θ diffractometer (D 5000 Siemens). The lattice constant 'a' for the cubic phase structure were determined by the relation

$$a^2 = \frac{\lambda^2(h^2 + k^2 + l^2)}{4\sin^2\theta}$$

(4.4)

4.4.2 Lattice Parameters

The lattice constant (or lattice parameter) refers to the constant distance between unit cells in a crystal lattice. Lattices in three dimensions generally have three lattice constants, referred to as *a*, *b*, and *c*. However, in the special case of cubic crystal structures, all of the constants are equal and it is only referred to *a*. Similarly, in hexagonal crystal structures, the *a* and *b* constants are equal, and it is referred to the *a* and *c* constants. A group of lattice constants could be referred to as lattice parameters. However, the full set of lattice parameters consist of the three lattice constants and the three angles between them.
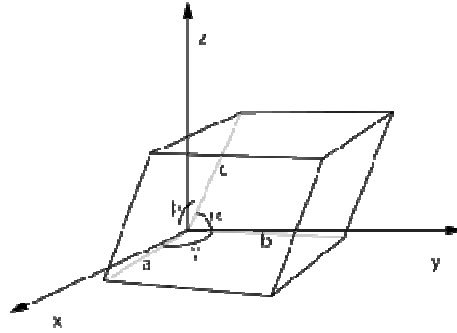
Figure 4.3 Unit cell definition using parallelepiped with lengths a, b, c and angles between the sides given by α, β, y.

Lattice parameter measurements are used in many situations to characterize materials. For example, knowledge of the lattice parameters can provide information on the thermal properties of a material, an indirect method to determine the compositions in a solid solution, a measure of the strain state, or an analysis of the defect structure.

Therefore, it is important to determine the lattice structure with the highest precision. Fortunately, X-ray diffraction can provide such information to an accuracy of several significant figures if care is taken during the experiment and subsequent analysis. If the crystal structure of a material is known, then the diffraction pattern can be indexed rather easily. However, in order to use this indexing to compute a precise value of the lattice parameter, careful analysis of the data is required. For example, in a cubic system, the *d* spacing corresponding to each diffraction line can be related to the lattice parameter a through

$$a^2 = \frac{d^2}{h^2 + k^2 + l^2}$$ (4.5)

where *hkl* are the Miller indices. If there are no systematic errors in the positions of the diffraction peaks, then there would be only random errors in the individual calculations of the lattice parameter. However, systematic errors occur for a number of reasons that require a sophisticated approach to compensate fully for such errors.

4.2.3 Grain Size

Grain growth refers to the increase in size of grains (crystallites) in a material. This occurs when recovery and recrystallisation are complete and further reduction in the internal energy can only be achieved by reducing the total area of grain boundary.

Grain growth occurs by the movement of grain boundaries and not by coalescence. Boundary movement is discontinuous and the direction of motion may change suddenly. When grain boundaries in a single phase meet at angles other than 120 degrees, the grain included by the more acute angle will be consumed so that the angles approach 120 degrees [88].

Grain boundary migration occurs when a shear stress acts on the grain boundary plane and causes the grains to slide. This means that fine-grained materials actually have a poor resistance to creep relative to coarse grains, especially at high temperatures, because smaller grains contain more atoms in grain boundary sites. Grain boundaries also cause deformation in that they are sources and sinks of point defects. Voids in a material tend to gather in a grain boundary, and if this happens to a critical extent, the material could fracture.

It is observed that the XRD patterns of all CuS thin films show a most preferred orientation along (102) plane. The grain size of the CuS thin films were estimated for the (102) plane by using the Scherrer formula.

$$d = \frac{\lambda}{Dcos\theta} \qquad (4.6)$$

where d is the grain size, λ is the X-ray wavelength used, D is the angular line width of the half-maximum intensity and θ is the Bragg angle [90].

4.2.4 Microstrain

Misfit stresses occur in crystalline films due to the geometric mismatch at interphase boundaries between crystalline lattices of films and substrate. Therefore, a stress is also developed in the film due to the lattice misfit. However, the stress has two components: thermal stress arising from the difference of expansion coefficient of the film and substrate and internal stress due to the accumulating effect of the crystallographic flaws that are built into the film during deposition. The average stresses of the deposited films are found to be compressional in nature. The compressive stress is due to the grain boundary effect, which is predominant in polycrystalline film. Compressive stress is also likely to be due to the native defects arising from the lattice misfit. Native imperfections probably migrate parallel to the film substrate with their surface mobility modified by the substrate temperatures. The origin of the strain is also related to the lattice misfit which in turn depends upon the

deposition conditions [89,90]. The microstrain (ε) developed in the sprayed CuS thin films were calculated from the Eq. 4.7.

$$\varepsilon = \frac{D cos\theta}{4}$$

(4.7)

where D is the full width at half maximum of the (102) peak.

4.2.5 Dislocation Density

Dislocations are an imperfection in a crystal associated with the misregistry of the lattice in one part of the crystal with respect another part. Unlike vacancies and interstitial atoms, dislocations are not equilibrium imperfections, i.e., thermodynamic considerations are insufficient to account for their existence in the observed densities. In fact, the growth mechanism involving dislocation is a matter of importance. In this study, the dislocation density is determined from Williamson's and Smallman's method using the following relation for cubic CuS thin films and the variation of the dislocation density with substrate temperature [90].

$$\rho = \frac{15\varepsilon}{aD}$$

(4.8)

CHAPTER 5
RESULTS AND DISCUSSION

5.1. Introduction

The spray pyrolysis technique is basically a chemical deposition technique, in which solutions of the desired material are sprayed onto a preheated substrate. Continuous films are formed onto hot substrate by thermal decomposition of the reactants. Films prepared by this technique are generally polycrystalline in structure and their properties are extremely influenced by the deposition process. In particular, spray pyrolysis has proved well suited for producing semiconductor films of the desired stoichiometry on large and non-planar areas.

5.2 The Determination of CuS Thin Film Thickness

The thickness of the films was determined using a micro gravimetrical method. The films were deposited on clean glass a slide that mass was previously determined. After the deposition the substrates it was again weighted, determining the quantity of deposited CuS. Measuring the surface of the deposited film, taking account of CuS specific weight of the film, thickness was determined using the relation:

$$t = \frac{(m_2 - m_1)}{\rho A} \qquad (4.1)$$

where A is the surface of the film (cm^2), m_{CuS} is the quantity of deposited cooper sulfide, and ρ is the specific weight of CuS (density of CuS=4.68 g/cm^3). The thickness measurement results are given in Table 5.1.

5.3 Effect of the Substrate Temperature on the Thin Film Formation

The depositions were carried out at substrate temperatures between 250 and 450^{0}C using spraying solution. Spraying the precursor solution at substrate temperature 250^{0}C resulted whitish opaque coating and the coated layer was less adherent to the substrate surface. CuS films formation did not occur until the

substrate temperature 250^0C due to insufficient thermal energy to decompose the precursor solution. It is observed that the lower substrate temperatures ($<350^0C$) result into a non-uniform and easily detachable film formation. The lower thermal energy available for the molecules in the solution at this lower deposition temperature can also cause incomplete reactions between the precursors on the surface of the substrate. And also the temperature may be insufficient in this case, to decompose the sprayed droplets of the mixed solution. At higher substrate temperatures ($>350^0C$), also non-uniform and easily detachable films result. This may be due to higher rates of evaporation of initial ingredients from the surface of the hot substrates. However, the films prepared at 350^0C substrate temperatures are uniform and good adherent to the glass substrates. With the increases of the substrate temperature, the quality of the formed films was improved. It is known that at high substrate temperature, the mobility of the ad-atoms is high and this fact promotes that the ad-atoms be able to diffuse reaching a nuclei and that desorption of product molecules from the surface be carried out. The experiments were performed at temperatures in the range 250 and 350^0C. Increase in crystallinity with substrate temperature is due to the optimum rate of supply of thermal energy for recrystallization with substrate temperature. Thus it is found that the best results were obtained at 350^0C.

5.4 XRD Studies of CuS Thin Films

The intensity of the XRD peaks was enhanced with the increase of the substrate temperature. Substrate temperature is one of the most important factors which affect the crystallization of films. The energy and the mobility of atoms on the surface of the substrate are dependent on the substrate temperature directly. High temperature means high energy and high atom mobility, which are all beneficial to crystallization. In order to study the effect of substrate temperature on the CuS phase formation, all films were characterized by using X-ray diffractometer. Fig. 5.1 and Fig. 5.2 shows the XRD patterns of CuS films sprayed at 250, 350 and 450^0C substrate temperatures using the Cu:S molar ratios of 1:1 and 1:2, respectively. It has been reported earlier that when thin films are deposited by spray pyrolysis the material is crystallization occurs during the annealing for temperatures and with the substrate temperatures above the film deposition temperature. From Fig. 5.1, 5.2, 5.3 and 5.4 it is clear that not only annealed films but also as deposited films were

polycrystalline in nature. All peaks have been identified and indexed from the known patterns of the standard data files. As seen from the Fig. 5.1, the intensity of CuS (102) peak increases with increasing the substrate temperature and the peak becomes narrower indicating an improvement of the crystallinity. This means that the grain size of the thin films increases with increasing substrate temperature. Other diffraction peaks, such as (101) and (103) are also detected indicating that the films are polycrystalline with a preferred orientation along the (102) direction. This suggests that crystallinity and the preferential orientation increases with the increasing substrate temperatures. The results show that CuS films crystallized in hexagonal structure as all recorded diffraction peaks are characteristic for the polycrystalline structure (Fig. 5.1). With the increases of the substrate temperature, the quality of the formed films was improved.

As seen in Fig. 5.1 and 5.2, the crstallinity of the films prepared at 250^0C substrate temperature worse than other films which prepared at 350^0C substrate temperature this behavior is due to the fact that at low substrate temperature the starting materials ($CuCl_2$) and undesired by-products (H_2O, thiourea, etc.) are present in the films, suggesting that the substrate temperature is not enough for completing the chemical reaction, e.g. the droplet hit on the hot substrate removing a lot of heat causing a partial decomposition of the starting materials. CuS thin films prepared at and above 250^0C are polycrystalline materials and present a single phase with a hexagonal structure. The unique feature of all the diffractograms is that they contain the characteristic CuS orientations along the preferred (102) plane.

Figure 5.1 X-ray diffractogram XRD patterns of sprayed films from the solution with the molar ratio Cu:S;1:1 at growth substrate temperatures of 250, 350 and 450^0C.

This preferred orientation remains predominant irrespective of the substrate temperature. The presence of other peaks such as (101) and (103) has also been detected but with substantially lower intensities. Intensity of (102) peak increases progressively as the substrate temperature changes 250^0C to 350^0C and then it decreases afterward for further increase in substrate temperature. The increase in (102) peak intensity from 250^0C to 350^0C temperature may be attributes to the continuous increase in film thickness from 64 nm to 74 nm. Decrease in (102) peak intensity after 350^0C might be ascribed to the fact that at these substrate temperatures, there is complete thermal decomposition of sprayed droplets before reaching hot substrate due to unsuitable thermal energy (higher) than required for perfect decomposition and subsequent recrystallization. This evolution can be interpreted by the fact that increase in the substrate temperature improve the

crystallization of films of CuS. However, at higher temperatures, the temperature effect yields to the formation of the defects in the film and can also lead to the deterioration of the structural quality of films. It has been reported that the preferred orientation of CuS film on glass substrate is affected by source compounds, growth parameters such as solution concentration, solution feed rate, spraying gas pressure, substrate temperature and solvents. The enhancement of the crystal structure at temperature above of 350^0C is due to growth of the films carried out by the low temperature spray pyrolysis process, the solvent vaporizes near to the surface substrate then the resulting solid melts and vaporizes and the vapor diffuses to the substrate which undergoes a heterogeneous reaction. It is known that at high substrate temperature, the mobility of the ad-atoms is high and this fact promotes that ad-atoms be able to diffuse reaching a nuclei and that desorption of product molecules from the surface be carried out.
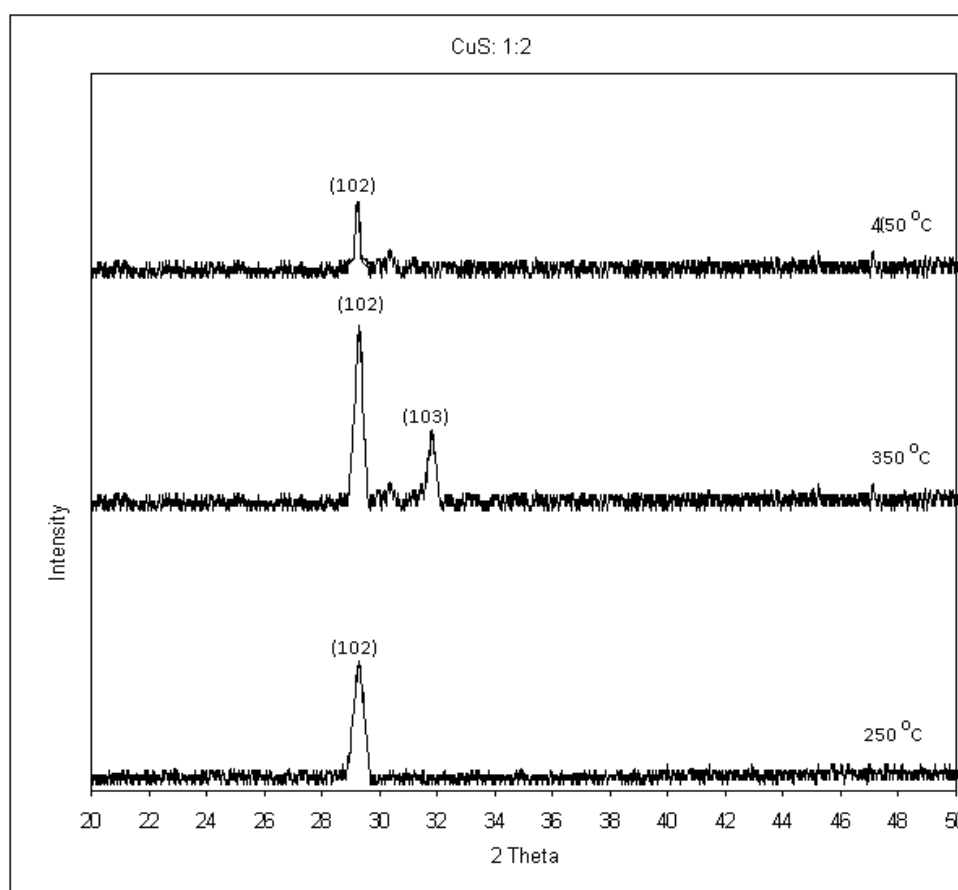
Figure 5.2 X-ray diffractogram patterns of sprayed films from the solution with the molar ratio of Cu:S;1:2 at growth substrate temperatures of 250, 350 and 450^0C.

In Fig. 5.2, the most intense diffraction peak from the CuS reference was observed at 29.25^0 and can be attributed to either the hexagonal (102) reflection. At a substrate temperature of 250^0C, the reflection at 31.80^0 arise from the hexagonal (103) plane. And the other reflection at 29.25^0 is possibly raised from the hexagonal (102) plane. The peaks shape indicates that the films have good crystallinity. At a substrate temperature of 350^0C, the XRD patterns show the hexagonal phase of the plane (102). Finally, CuS films grown from 1:2 solution at 250 and 350^0C substrate temperatures crystallize in polycrystalline structure as proved by distinct appearance of the (102) and (103) peaks of hexagonal crystal structure (Fig. 5.2). Thus it can be seen that the crystallites in the film are (102) orientated. This means that the preferential orientations of crystal growth are strongly dependent on the substrate temperature.
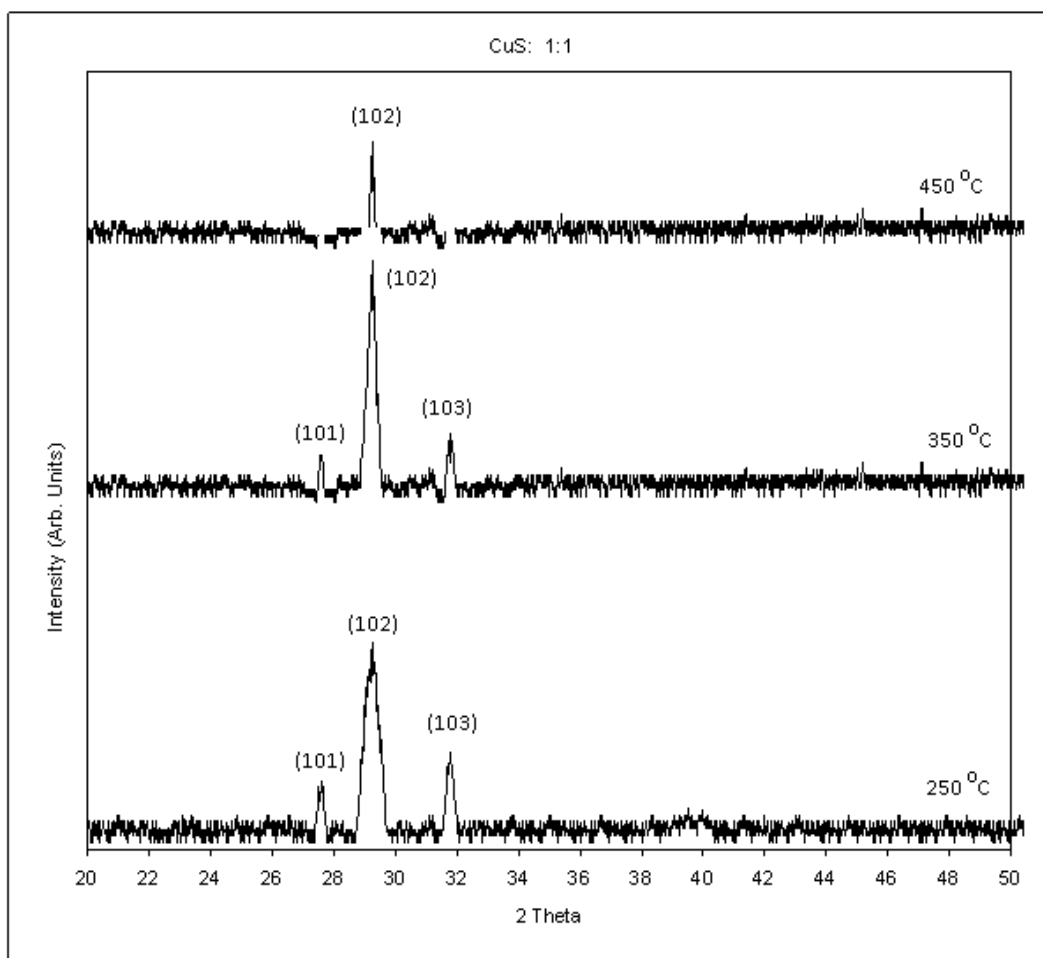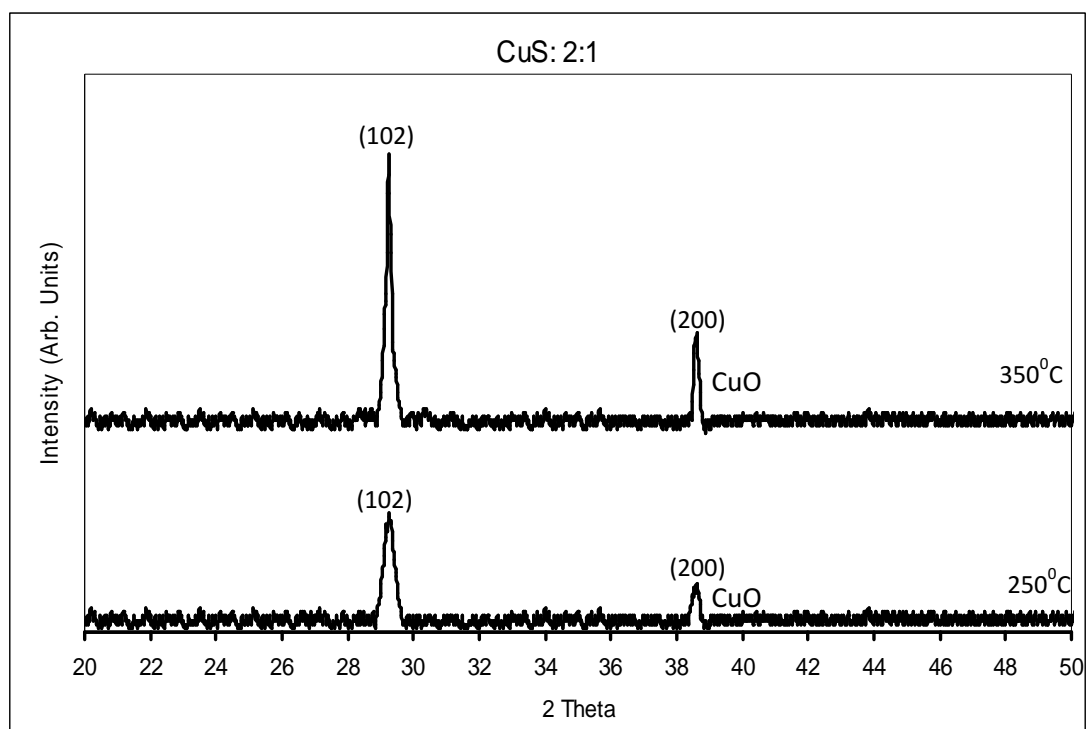

Figure 5.3 X-ray diffractogram patterns of sprayed films from the solution with the molar ratio of Cu:S;2:1 at growth substrate temperatures 250 and 350^0C.

The films were also deposited from Cu-rich solutions using Cu:S molar ratio of 2:1. The XRD pattern of the CuS films deposited at 250^0C substrate temperature in Fig. 5.3 shows a mixed pattern of CuS and CuO, indicating that there was a phase transformation from CuS to CuO. This implies that some sulfur sites are replaced by oxygen in the films. As the T_S is increased to 350^0C, CuO peaks are increased with

substrate temperature and CuS diffraction peaks only appear with a preferential (102) orientation. This means that CuS film can be converted partially to the CuO phase. These cause the deterioration of crystallinity of the CuS films. Consequently both, the deposition temperature and molar ratio of precursors have the effects on the crystallization in sprayed CuS thin films. Therefore it is shown that the intensity of the XRD peaks was enhanced with the increase of the substrate temperature. Substrate temperature is one of the most important factors which affect the crystallization of films. The energy and the mobility of atoms on the surface of the substrate are dependent on the substrate temperature directly. High temperature means high energy and high atom mobility, which are all beneficial to crystallization.

The polycrystalline structure of the CuS thin films has been revealed from the X-ray diffraction patterns confirms this property. Fig. 5.1, 5.2 and 5.3 shows the XRD images for three films deposited at different substrate temperatures 250, 350 and 450^0C. The difference between the three images was apparent especially those of the lower substrate temperature, where the density of grains and the grain size were larger at the higher substrate temperature which is consistent with the afore-mentioned results of the X-ray diffraction patterns. The narrowing of the lines of crystal grow that the higher substrate temperature means that the grain size had increased. The difference in the grain size became less apparent at the higher substrate temperature, which means that the rate of increase in grain size becomes slower. This result is consistent with the behavior of the crystallinity of the films, due to this process, coherent growth with the underlying grains do well proceed and new grains are nucleated on the top of the preceding ones. Increase in crystallinity and crystallite size with substrate temperature is due to the optimum rate of supply of thermal energy for recrystallization with substrate temperature. The values of crystallite size for different substrate temperatures are shown in Table 5.1.

Table 5.1 Structural parameters of spray deposited CuS thin films within substrate temperature and molar ratio.

	Substrate Temperature							
	250^0C			350^0C			450^0C	
CuCl$_2$	1	1	2	1	1	2	1	1
Thiourea	1	2	1	1	2	1	1	2
Grain Size (Å) (102)-plane	8.219	7.196	6.279	9.432	8.099	7.473	7.522	6.133
Thickness(nm)	64	50	48	74	62	56	55	44

As seen in Table 5.1, the grain sizes of the samples increased and FWHM decreased as substrate temperature increasing, implying that the crystallization degree was improved with the rising substrate temperature because the rising substrate temperature improved the mobility of the deposited atoms. We expect that this increase in grain size could not continue with increasing substrate temperature, but it reaches a certain value after which no further increase occurs. Also the crystallite size of all films increased initially with the increase of substrate temperature and reached a maximum value at 350^0C and became more or less constant afterwards. The increase in grain size with the growth temperature could be attributed to the enhanced reaction kinetics among the sprayed droplets as well as improvement in the ad-atom mobility on the substrate surface. The decreasing trend of grain size with the increase of strain due to the retarded crystal growth as the stretched lattice increases the lattice energy and diminishes the driving force for the grain growth in the sprayed CuS films.

5.5 Annealing of the CuS Thin Films

CuS film is known to exist in the hexagonal crystallographic forms. Fig. 5.4 shows the XRD spectrum of sprayed CuS film on a substrate heated at 350^0C using the Cu:S molar ratio of 1:1. This film is crystallized as hexagonal type with a strong peak corresponding to the (101), (102) and (103) directions, respectively. All deposits show this preferential orientation. Therefore, the as-deposited film showed a main diffraction peak at $2\theta = 29.25^0$, corresponding to the (102) diffraction of the hexagonal CuS film.

It is well-known that post-annealing is an important method to improve crystal quality. For the annealing process, the dislocations and other defects arise in the material and adsorption/decomposition occurs. Fig. 5.5 shows that the intensity of (102) reflection increases with the annealing temperature. It is attributed that this increase of peak intensity to the enhancement of clusters, rearrangement of atoms and removal of residual stresses/defects formed during the film deposition. It can be seen that sprayed CuS films shows sharp XRD reflection peak detected at 29.25^0, suggesting that the growth is along the c-axis normal to the substrate. The intensity of the peaks relative to the back ground demonstrates high purity of the hexagonal CuS phase and good crystallinity of the samples. The XRD patterns from the as-grown CuS film and annealed at 250^0C (Fig. 5.5) indicate a (102)-preferred orientation, which suggests that the film is aligned with the c-axis oriented perpendicularly to the substrate surface.

Figure 5.4 X-ray diffractogram of CuS film sprayed at 350^0C substrate temperature and annealed for 90 min. at 250^0C (Cu:S;1:1).
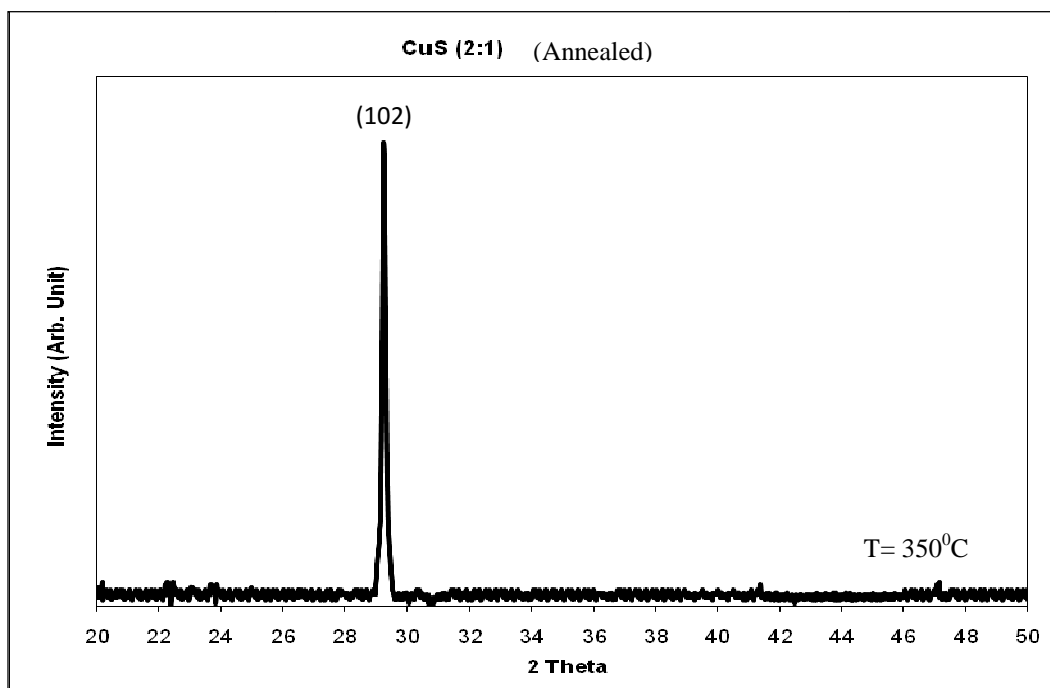
Figure 5.5 X-ray diffractogram of CuS film sprayed at 350^0C substrate temperature and annealed for 90 min. at 250^0C (Cu:S;2:1).

In Fig. 5.5, the strongest detected (hkl) peak was observed at 2θ values of 29.25^0, corresponding to the lattice plane (102) in CuS, indicating that a small amount of sulfur had entered the lattice of CuS and substituted some oxygen contents. The annealed samples show that as temperature increases the intensity of dominant peaks increases and width decreases. With further annealing process, oxygen atoms obtained enough kinetic energy to leave their lattice sites by thermal disturbance and sulfur atoms diffused into the CuS lattice to occupy the oxygen vacancies. It is clear that the strong peak intensity of XRD patterns increases with the annealing treatment, which means that this treatment leads to an improvement in the crystallinity of the films. It can be concluded that the highest changes were observed in the films with annealing. These results could be related to the decrease in the defect density due to the oxygen chemical desorption mechanism at grain boundaries, which is more significant when the annealing is performed at annealing temperature (250^0C). With the annealing temperature, the intensity of (102) peak increased while the intensity of other peaks unannealed films is very less, which indicates that the layers annealed at 250^0C showed better crystallinity than the layers unannealed films. Initially, there were many crystallites present in the as-deposited films that exhibited less intense peaks and when the layers were annealed at a

66

particular temperature, the small crystallites grew into larger ones with an improved crystallinity. The observed structural changes were attributed to the coalescence induced grain growth during the annealing process where smaller nuclei could easily rotate compared to the larger nuclei in order to minimize the interfacial energy. Therefore, it can be said that with annealing temperatures, the atoms have sufficient thermal energy to move into stable positions, so that structural reorientation occurs, leading to a significant increase in the intensity of (102) plane.

In general, the FWHM of 2θ values are related to the grain size of the film that the FWHM of the (102) diffraction peak is inversely proportional to the grain size of the film. Thus, smaller FWHM means larger the grain size and better the crystal quality of the film. From Fig. 5.5, it can be seen that the intensity as well as full width-half-maximum (FWHM) of (102) peak is dependent on annealing temperatures and the film remains highly oriented with the c-axis normal to the substrate. Also the intensity of the (102) diffraction peak becomes stronger and there is decreasing full width at half maximum (FWHM), meaning an improvement in the crystallinity and larger crystallite size of the films can be obtained. Thus it can said that the FWHM of XRD depends on the crystalline quality of each grain and the distribution of grain orientation. The increase of crystallite size with the increase of annealing temperature is mainly due to coalescence of smaller nuclei or neighboring grains resulting in the improvement of crystallinity. And it may be due to the removal of defect levels after heat treatment, which is frequently observed in films prepared using spray pyrolysis methods. Major improvement in the grain size was observed by annealing the layers. The results obtained from XRD studies revealed that the crystalline quality of the film grown at $350^{0}C$ substrate temperature can be greatly improved through annealing. And also it is shown that crystallinity of the film was found to increase with increase in substrate temperature and annealing temperature.
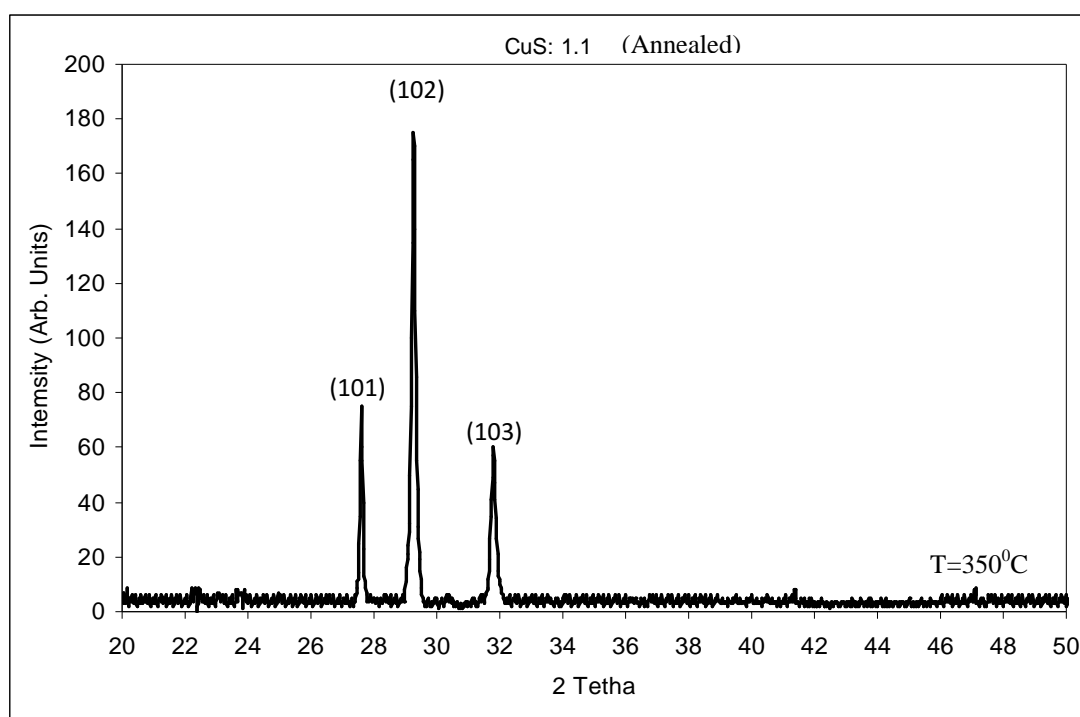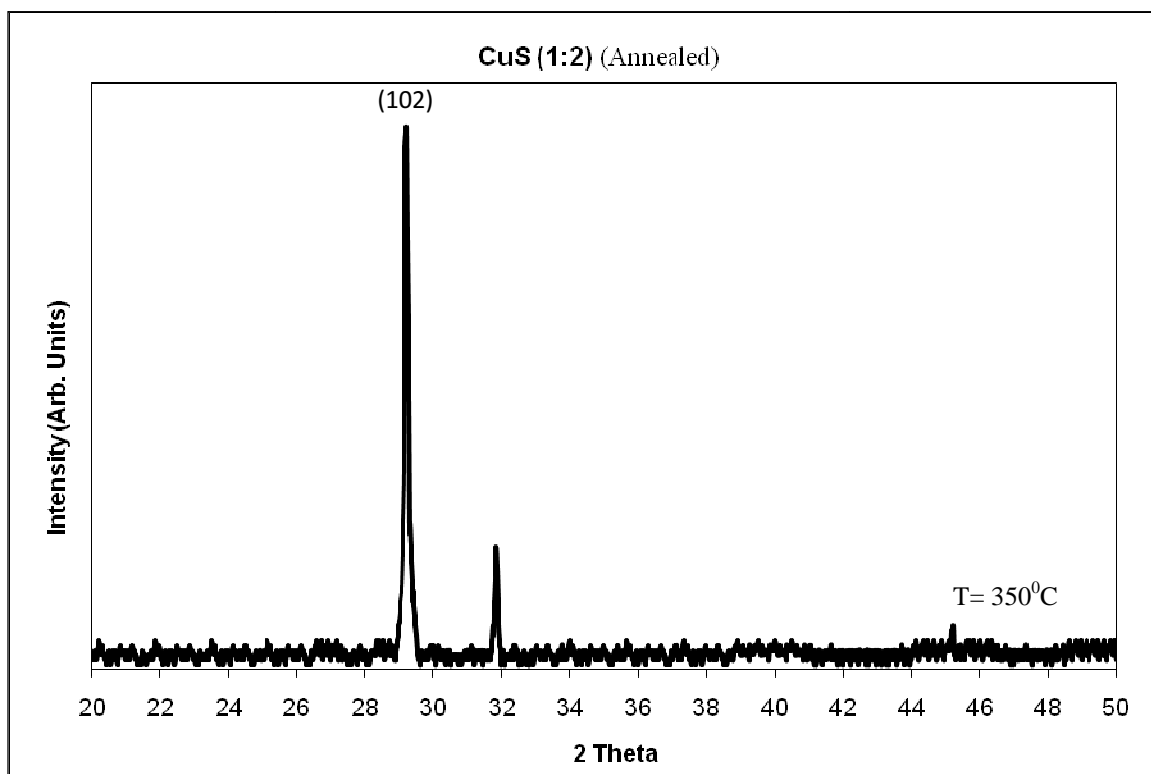
Figure 5.6 X-ray diffractogram of CuS film sprayed at 350^0C substrate temperature and annealed for 90 min. at 250^0C (Cu:S;1:2).

## 5.6 Optical Properties of the CuS Thin Films

The optical properties of the investigated samples were studied by the method of the spectral optical transmission. All the films show the transparency and good adherence to the substrate. As the examination is done for the film-substrate combination, the transmission of the substrates is also measured and subtracted. Fig. 5.7 shows the transmittance of CuS films prepared at various substrate temperatures with the ratio Cu:S;1:1. It can be seen that the optical transmission improves when the substrate temperature increases. This may be due to the decreased optical scattering caused by the decrease of grain boundary density owing to the increase of grain size. The film deposited at the substrate temperature (T_S=350^0C) shows an optical transmittance above 74% in the visible region with a steeper optical absorption curve, which indicates a relatively better crystallinity and lower defect density near the band edge.
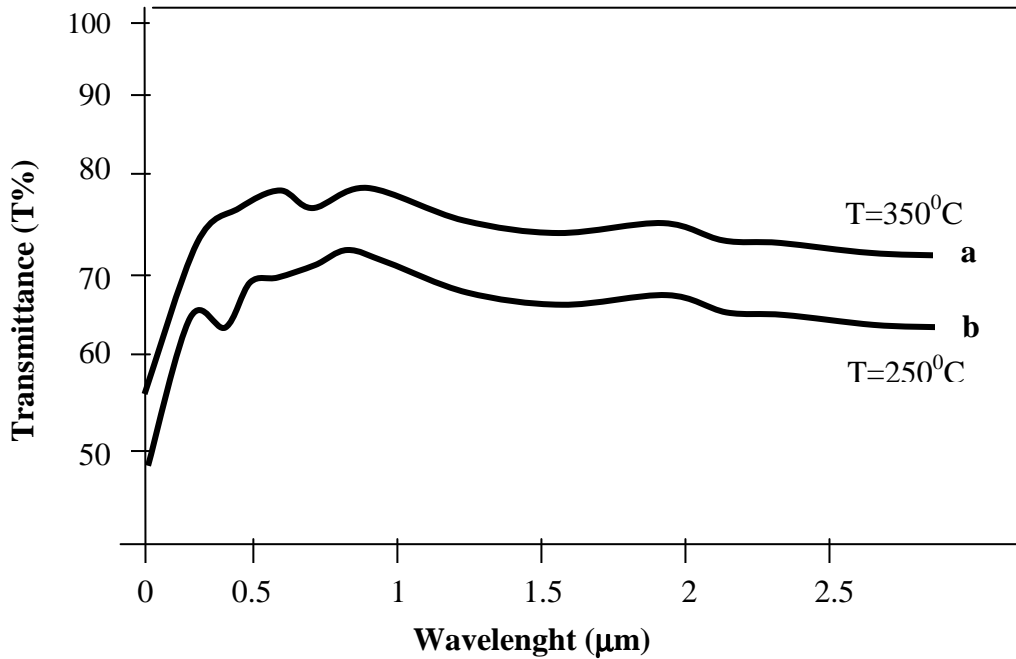
Figure 5.7 Transmittance versus wavelength for CuS films prepared at various substrate temperatures: (**a**) $T_S=350^0$C; (**b**) $T_S=250^0$C.

From this spectrum an abrupt absorption edge at 600 nm can be seen, which is characteristic of a material with a direct energy band gap (E_g). It can be seen that, the transmittance spectra for all samples has been divided into three special regions: (i) the strong-absorption region (a lowering of about 40% in transmittance), where λ is typically smaller than 600nm; (ii) the transparent region, where λ is typically higher than 2000 nm and (iii) the absorption region between the two latter regions. Also, the obtained spectra of the CuS films are characterized by the typical semiconductor material with good optical quality. The observed higher transmittance at the substrate temperature 350^0C could be due to less scattering effects, improved structural homogeneity and better crystallinity while its decrease at low substrate temperature 250^0C was due to the stoichiometric deviations. And the interference peaks present in each spectrum confirm that the films are uniform. The sudden fall of transmission below 500 nm is most probably due to the absorption edge. The films prepared at 250^0C substrate temperature show less transmittance at shorter wavelengths, whereas film prepared at 350^0C substrate temperature revealed higher transmittance. The variation in absorption edge most probably due to the improvement in structural order, removal of residual stresses and quantum confinement effects. This behavior is probably due to the increase in the crystallite

size. It is known that intercrystallite boundaries, being highly disordered and a sink for impurities can have properties very different from those of the crystallites giving a marked contribution to the optical transmittance of the thin films. Thus the increase in transmittance with substrate temperature is attributed to the improvement of crystallinity and stoichiometry as shown by XRD.

From the absorbance data, the absorption coefficient (α) as a function of the photon energy was calculated and plotted for the direct allowed transition by using formula:

$$(\alpha h v)^2 \alpha h v - E_g \qquad (5.1)$$

where E_g is the transition energy gap and hv is the photon energy. It can be observed that the absorption coefficient increases exponentially with increases of photon energy. The variation of α with hv can be attributed to the optical scattering at the grain boundaries and the intrinsic absorption due to high concentration of defect states in the grain boundaries. The optical band gaps computed from the above relation are estimated to be 2.38, 2.10 and 2.35 eV for films obtained at substrate temperature of 250, 350 and 450^0C, respectively. It is found that the band gap energy is decreased from 2.38 eV to 2.10 eV as the deposition temperature was increased from 250^0C to 350^0C. This behavior indicates that when the substrate temperature was increased, the band gap shifted to a lower energy value with the increase in deposition temperature and transmittance. Theoretically, the decrease of optical band gaps is related to the volume change with temperature and electron-phonon interaction. As the films were deposited at higher temperature, the crystallites began to move and tended to agglomerate easily. As a result, the band gap of crystallites decreases with increasing substrate temperature, which indicates that crystallization, would cause the E_g narrowing. It could be explained by crystalline state improvement with increasing the substrate temperature. Also, the shift observed at absorption edge toward lower photon energies for thin films deposited on heated substrates could be attributed to the increase in crystallite size and change in the stoichiometry due to loss of oxygen, resulting in the formation of shallow acceptor levels in the forbidden band of CuS thin films. It is clearly seen that with increasing substrate temperature up to 350^0C, the E_g of the films is broadened and the grain size increases. This is explained by the fact that the free electrons are trapped at grain boundaries. When the

grain size increases, the density of grain boundaries decreases and as a result fewer carriers are trapped in the space charge region, leading to a higher amount of free carriers. It is observed that the substrate temperature mostly affects the band gap of the films. Then the band gap energy is increased to 2.35 eV as the deposition temperature was increased to 450^0C. It is indicates that the energy band gaps, for CuS films increase with increasing substrate temperature while microstrain increases and grain size decreases. Thus it can be said that the microstrain in the films causes an increase of the bandgap. The compressed lattice is expected to provide a wider band gap because of the increased repulsion between the sulphur 2p and the copper 4s bands.

This results show that the variation of grain size with energy band gap, substrate temperature and microstrain. A dependence of band-gap energy shift on the grain size is attributed to a electron confinement effect related with the grain size in the films. It was observed that when the grain size was increased, the band-gap shifted to a lower energy value and the decrease microstrain. Also, shift observed at absorption edge toward lower photon energies for the films deposited on heated substrates could be attributed to the increase of crystallite size and change of the stoichiometry of the films, resulting in the formation of shallow acceptor levels in the forbidden band of CuS films. Therefore, the thickness can cause increase of the grain size which decreases the apparent energy gap. The decrease of the energy gap by the grain size will be due to diminishing of the quantum size effect. This means that the size of the cluster of grains composing the as-deposited film is small enough to cause the quantum effects. From the results of structure analysis, it is apparent that the optical band gap decreases with the decrease of defects and with the increase of grain size. Since microstrain is the manifestation of dislocation network in the films, the decrease of microstrain indicates a decrease of the concentration of lattice imperfections and the formation of high quality films with increasing grain size and improvement in the crystallinity with less defects. The change of energy band gap and lattice strain with grain size could infer that the lower the lattice strain, the lower the energy band gap. This implies that lattice strain in the films restricts the growth of grains. This may come from the retarded crystal growth due to the stretched lattice that can increase the lattice energy and diminishes the driving force of the growth. As a result, the crystallite size of CuS films can be influenced by factors such as defects,

impurities, microstrain, energy band gap and thickness. Also, it can be seen that the band gap decreases as the film thickness increases. This decrease of the band gap can be due to the influence of various factors such as grain size, structural parameters, presence of impurities, and deviation from stiochiometry of the film and lattice strain. Therefore, it is observed that the grain size and the strain have a direct dependence on the film thickness. As a result, the observed decrease in E_g and microstrain with increasing grain size could be attributed to the improvement of the crystallinity.

Fig. 5.8(a) and (b) shows the $(\alpha h\nu)^2$ versus $h\nu$ plots of CuS film deposited at 350^0C substrate temperature with the ratio 1:2, 2:1 and 1:1 unannealed and annealed, respectively. The stoichiometry of the thin films is improved, i.e. , the defect number decreases with annealing treatment and the light loss due to the scattering of defects centers decreases resulting in the increase of the transmittance. Annealing treatment can increase the homogeneity and crystallinity of the structure of the films and decrease the defect density at the edge of energy band gap. From Fig. 5.8 (a) and (b), the plots of $(\alpha h\nu)^2$ versus $h\nu$ indicate that there is some tailing in the band gap below the absorption edge. This means that there is a high concentration of impurity states in the thin films which can cause a perturbation of the band structure with the result that the parabolic distribution of the states will be disturbed by a prolonged tail into the energy gap. The tails in the optical spectra of the thin films could be due to the broadening of the impurity levels and their spatial overlap into a band. At high concentrations, the impurity band merges with the nearest intrinsic band. Due to this, the Fermi Level will lie inside the parabolic portion of the appropriate band. Thus, less activation energy will be needed for the electrons to move from the Fermi Level into the conduction band. The tails could also be due to ionized donors which could exert an attractive force on the valence band. Thin films were deposited at 350^0C substrate temperature and annealed at 250^0C in air for 90 min. The direct gap values for different Cu:S ratios and annealed and unannealed thin films were listed in Table 5.2. It was observed that E_g is depended on the Cu:S ratios. The optical band gap of CuS film decreased with the annealing temperature, the minimum optical band gap of CuS film reached to 1.95 eV at an annealing temperature of 250^0C. The temperature dependent parameters that affect the band gap are reorganization of the film, selenium evaporation and self oxidation of the film. The reorganization of the

film should occur at all annealing temperatures. By filling the voids in the film one expects denser films and smaller energy gaps. The decrease in band gap after heat treatment for CuS films may also be attributed to the quantum confinement of the charge carriers in very fine nanocrystalline grains. A characteristic of the film that is affected from its crystallinity is the optical band gap. It is obvious that the optical bandgap decreases when the grain size increase. Thus, crystallization via nucleation and growth becomes possible and depends on the annealing temperature. Also, the crystallization of the CuS films increases with the annealing temperature. It may be due to reduction in the grain boundary scattering, when crystalline size increases, which supports the XRD results. As the thickness increases, the band gap energy decreases, which may be attributed due to grain growth and increase of localized grain boundary, which in turn increases the point defects. The most important influence of the annealing process on the optical characteristics is related to recrystallization of the CuS crystallites. Changes in the bandgap energy with annealing temperature can be associated to changes in the lattice parameter, induced strains due to thermal expansion and to size growth of the crystallites. The bandgap energy decreases when the lattice parameter decreases when the size of the crystallites increases. And also the decreased band gap after annealing is due to the improvement in the crystalline nature of the material. The authors reported two main reasons for this behavior. The first reason of the direct band gap shift was the effect of the lattice changes, which relates to the change of electron energies with the volume. The second reason was the direct renormalization of the band energies due to the temperature dependence of the electron-phonon interactions.

Generally in polycrystalline semiconductors, the energy band gap can be affected by the stoichiometric deviations, quantum size effect, change in preferred orientation of the films, dislocation density and disorder at the grain boundaries. The decrease of energy band gap with annealing temperatures could be due to the formation of localized states in the band gap region. These states might be induced in the band gap because of the structural disorder due to the sulfur deficiency. This high concentration of impurity states cause the band structures to perturb, resulting in a prolonged tail extending in to the energy band gap. The width of the band tails, known as Urbach tails, was evaluated to quantify the structural disorder. Moreover, the energy band gap could also be influenced by the variation of particle size with

annealing temperature as it is in the nanometer range. Therefore in the present study, both the stoichiometric deviations and improvement in the particle size could contribute to the decrease of energy band gap in the films with the annealing temperature.
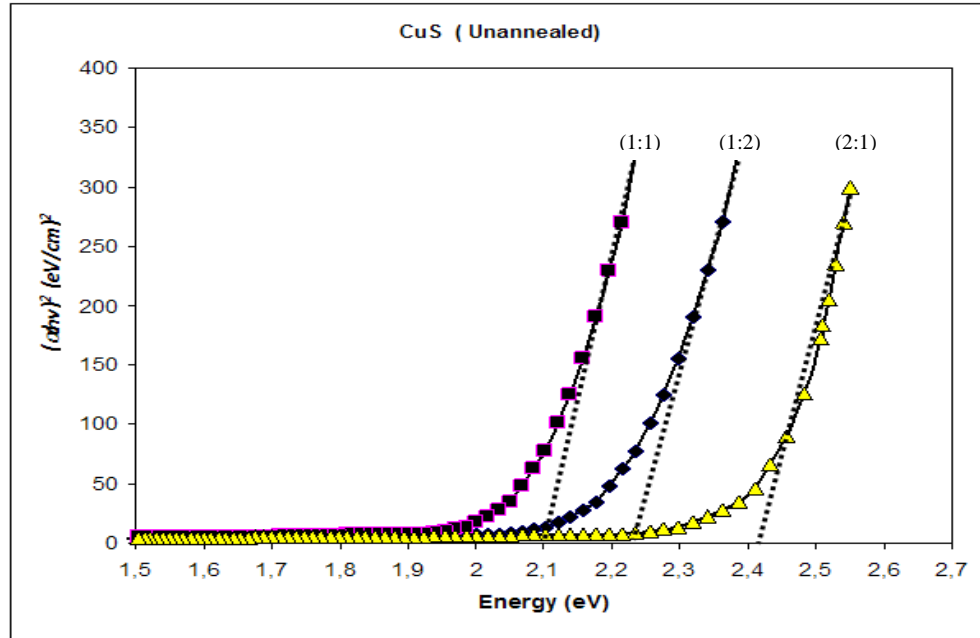
(a)

Figure 5.8 (**a**) The $(\alpha h v)^2$ versus hv plot of unannealed CuS film with the 1:2, 2:1 and 1:1 ratio at substrate temperature 350^0C.
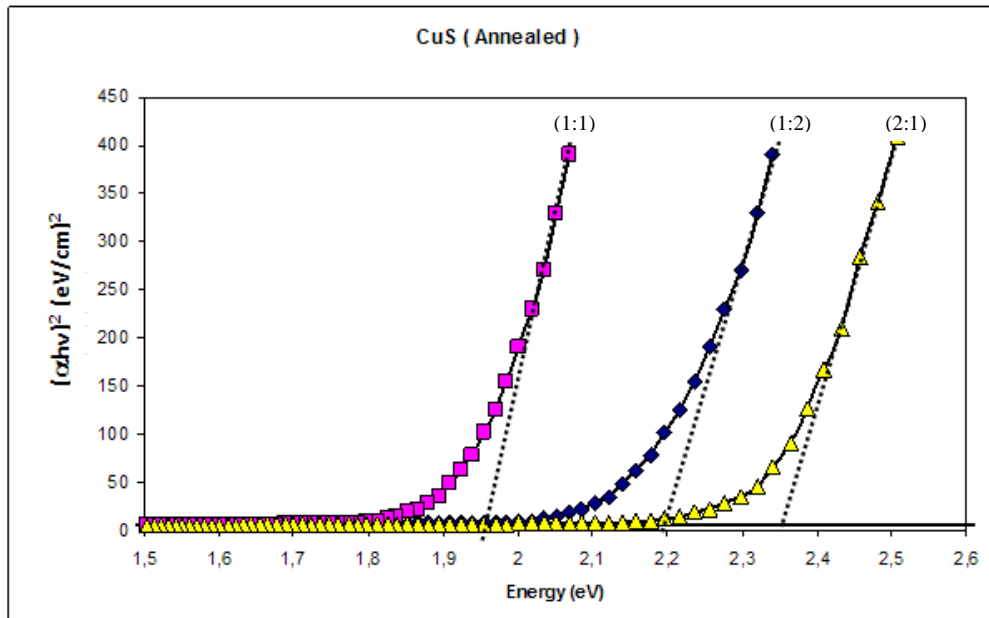
(b)

Figure 5.8 (**b**) The $(\alpha h v)^2$ versus hv plot of annealed for 90 min. at 250^0C CuS film with the 1:2, 2:1 and 1:1 ratio at substrate temperature 350^0C.

Table 5.2 estimated band gap E$_g$ and activation energy for different Cu:S ratios in CuS films deposited at 350^{0}C substrate temperature with annealing for 90 min. at 250^{0}C.

Table 5.2 The bandgap energy values of CuS thin films without annealed and annealed.

Sample Number	Cu:S Ratio	Without annealed thin films 'E$_g$' (eV)	Annealed thin films 'E$_g$' (eV)
1	1:2	2.28	2.20
2	2:1	2.41	2.35
3	1:1	2.10	1.95

It is observed from these results, the optical absorption measurements indicate that the absorption mechanism is due to direct transitions for the as-deposited and annealed films. The corresponding values of optical energy gap E_g are found to decrease with the annealing treatment due to the improved crystallization of the films, can be attributed to an increase in the of thermally induced crystalline phase. Therefore, there are two possibilities to improve the crystallinity of the films; the increase of the grain size to decrease the number of grain boundaries; the decrease of the barrier height at the grain boundaries.

The XRD data are also used for the calculation of the lattice constant, the crstallite size, the microstrain and the dislocation density. Table 5.3 shows the crystallite size, the microstrain, the dislocation density and lattice constant associated to the (101), (102), (103 and (200) peaks. From these results, we can see that the fundamental effect of the substrate temperatures and solution concentrations is related to an increase in the size of the crystallites and a decrease in the lattice parameter, dislocation density and the microstrain. This behavior shows that the strain and dislocation density decreases, whereas grain size increases with the increase of substrate temperature, which indicates the improvement in crystallinity of the films. And data shows that the lattice constant of the films deviates which indicates that crystallites of films are under strained that may be due to the change in nature and concentration of the native defects. Also the decrease in the value of the

lattice constant as substrate temperature and solution concentration is raised may be attributed to the re-orientation of the crystallites in the preferable direction.

From the datas, it can be understood that microstrain in the film is tensile. It decreases with variation of solution concentrations, indicating existence of more relaxed films for the ratio of Cu:S;1:1. This means that the crystallinity becomes better in the the ratio of Cu:S;1:1 films. The grain size increases with substrate temperature increases. As deposition temperature increases up to $350^{0}C$, amount of solute (i.e. Copper chloride) reaching on the surface of the substrate increases to form film and therefore the electrostatic interaction between solute particles becomes larger thereby increasing the probability of more solute particles to be gathered together forming a grain. Thus as the thickness increases, grain size also increases, which also indicates the improvement in crystallinity of the films.

Table 5.3 Some crystal structure parameters of the samples with respect to the substrate temperature.

CuS (1:1)	(hkl)	Lattice Constant (A)	Grain Size (A)	Microstrain	Dislocation Density
Substrate Temperature (T=450^{0}C)					
	102	5.713	7.522	8.769	7.971
CuS (1:2)					
	102	5.013	6.133	8.973	8.191
Substrate Temperature (T=350^{0}C)					
	101	4.567	8.126	0.0421	0.7972
	102	5.825	5.132	0.0627	0.5312
	103	6.730	6.167	0.0579	0.4027
CuS (1:2)					
	102	6.763	5.499	0.07463	0.53158
	103	8.883	7.697	0.08654	0.4974
CuS (2:1)					
	102	6.825	7.973	0.0387	0.5317
CuO	200	4.665	6.173	0.0519	0.758
Substrate Temperature (T=250^{0}C)					
	101	4.926	9.238	0.0586	0.8321
	102	6.823	7.119	0.06129	0.4427
	103	8.781	8.017	0.08910	0.5763
CuS (1:2)					
	102	6.192	6.096	0.11251	0.7123
CuS (2:1)					
	102	7.129	8.279	0.1064	0.6174
CuO	200	5.917	7.917	0.0889	0.7691

It is observed from Table 5.3 that the microstrain of the the ratio of CuS;1:1 exhibits a slow increasing trend up to the value of the (101) and (103) peaks from the data of the (102) peaks with the substrate temperatures. This type of change in microstrain may be due to the predominant recrystallization process in the polycrystalline thin films and due to the movement of interstitial Cu atoms from inside the crystallities to its grain boundary which dissipate and lead to a reduction in the concentration of lattice imperfections. Dislocation density is defined as the length of dislocation lines per unit volume of the crystal. Also it can be seen that the dislocation density similarly gradually decreases with the peaks of the XRD results at the ratio of CuS;1:1 as like the above results, it is evident that a good thermal treatment can largely decrease the film dislocation density and improve its crystallization. It is observed that the variation of dislocation density and microstrain generated in films with solution concentration. It is seen that, as solution concentration of the Cu increases or decreases the dislocation density and microstrain generated in the films increases. Due to the fewer defects in the lattice, the microstrain in the films gets released and minimum value of microstrain is obtained for films prepared the solution concentration of Cu and S is the same thin films with lower strain and dislocation density improve the stoichiometry of the films which in turn causes volumetric expansion of films. Therefore it can be said that the variation of crystallite size, microstrain and dislocation density with respect to solution concentration of the $CuCl_2$ and thiourea is the same, represents that the microstrain and dislocation density decreases whereas the crystallite size increases.

Table 5.3 shows that the lattice constant, microstrain and dislocation density of the samples decreases with the increasing substrate temperature, which is the indication of typical semiconductor characteristics. The decreasing may be due to the increasing the crystallite size of the samples. This behavior may also be attributed to the nanocrystalline nature of the thin films crystallite boundary discontinuities, presence of surface states, thickness of the films, the change in structural parameters and removed of some impurities. Also, the presence of a number of defects such as structural dislocations, disorders and surface imperfections play a role in decreasing lattice constant, microstrain and dislocation density.

The results observed that the microstrain in the film introduced by impurities, defects and lattice distortions in the crystal, and by the lattice mismatch between the

film and substrate. It shows that the measured film microstrain is mainly caused by the growth process itself. It suggests that the microstrain is generated during deposition due to the freezing of structural defects at low substrate temperature. The increase in substrate temperature increases the atomic mobility and reduces the structural defects, and thus a relaxation of CuS films is observed. The films deposited at lower substrate temperature exhibits strong microstrain. But for a CuS thin film grown at higher substrate temperature, the microstrain quickly relaxed due to the high kinetic energy of growing CuS. From Table 5.4, one can see that microstrain decreases with increase in substrate temperature. Where as the samples prepared at 350^0C show a small increase in microstrain. This may be attributed to the film thickness variation or crystallite size of the film and improvement of the films.

Table 5.4 Some crystal structure parameters of the samples which are annealed at $T_{an}=250^0C$.

ANNEALED ($T_{an}=250^0C$)					
Substrate Temperature ($T=350^0C$)					
CuS (1:1)	(hkl)	Lattice Constant (A)	Grain Size (A)	Microstrain	Dislocation Density
	101	4.012	9.396	0.0221	0.4852
	102	4.537	8.317	0.0627	0.3936
	103	5.463	7.963	0.0579	0.3287
CuS (1:2)					
	102	5.243	7.338	0.06124	0.41478
	103	6.371	7.982	0.05321	0.4071
CuS (2:1)	102	3.515	9.104	0.0387	0.4532

Table 5.4 shows the crystallite size, the microstrain, the dislocation density and lattice constant associated to the (101), (102) and (103) peaks. From these results, it is seen that the fundamental effect of the annealing and solution concentrations is related to an increase in the size of the crystallites and a decrease in

the lattice parameter, dislocation density and the microstrain. This behavior shows that the strain and dislocation density decreases, whereas grain size increases with annealing, which indicates the improvement in crystallinity of the films. And data shows that the lattice constant of the films deviates which indicates that crystallites of films are under strained that may be due to the change in nature and concentration of the native defects. Also the decrease in the value of the lattice constant as annealing and solution concentration is raised may be attributed to the re-orientation of the crystallites in the preferable direction.

From the datas, it can be understood that microstrain in the film is tensile. It decreases with variation of solution concentrations, indicating existence of more relaxed films for the ratio of Cu:S;1:1. This means that the crystallinity becomes better in the the ratio of Cu:S;1:1 films. The grain size increases with annealing.

CHAPTER 6
CONCLUSION

The purpose of this study is to prepare CuS films under the different conditions using the spray method. Firstly, a non-uniform and easily detachable film formation was observed at lower substrate temperatures $(Ts<350^0C)$ and at higher substrate temperatures $(Ts>350^0C)$. The lower thermal energy available for the molecules in the solution at this lower deposition temperature can also cause incomplete reactions between the precursors on the surface of the substrate. However, the films prepared at 350^0C substrate temperatures are uniform and good adherent to the glass substrates and the quality of the formed films are improved. It is found that the best results of the film formation were obtained at 350^0C.

The intensity of the XRD peaks was enhanced with the increase of the substrate temperature. Substrate temperature is one of the most important factors which affect the crystallization of films. The intensity of CuS (102) peak increases with increasing the substrate temperature and the peak becomes narrower indicating an improvement of the crystallinity. This means that the grain size of the thin films increases with increasing substrate temperature. Other diffraction peaks, such as (101) and (103) are also detected indicating that the films are polycrystalline with a preferred orientation along the (102) direction. This suggests that crystallinity and the preferential orientation increased with the increasing substrate temperatures. The results show that CuS films crystallised in hexagonal structure as all recorded diffraction peaks are characteristic for the polycrystalline structure. With the increases of the substrate temperature, the quality of the formed films was improved.

It can be seen that the crystallites in the film are (102) orientated. This means that the preferential orientations of crystal growth are strongly dependent on the substrate temperature. The grain sizes of the samples increased and FWHM decreased as substrate temperature increasing, implying that the crystallization

degree was improved with the rising substrate temperature because the rising substrate temperature improved the mobility of the deposited atoms.

It is well-known that post-annealing is an important method to improve crystal quality. The annealed samples show that as temperature increases the intensity of dominant peaks increases and width decreases. It is clear that the strong peak intensity of XRD patterns increases with the annealing treatment, which means that this treatment leads to an improvement in the crystallinity of the films. It can be concluded that the highest changes were observed in the films with annealing. These results could be related to the decrease in the defect density due to the oxygen chemical desorption mechanism at grain boundaries, which is more significant when the annealing is performed at annealing temperature (250^0C). With the annealing temperature, the intensity of (102) peak increased while the intensity of other peaks unannealed films is very less, which indicates that the layers annealed at 250^0C showed better crystallinity than the layers unannealed films.

The optical properties of the investigated samples were studied by the method of the spectral optical transmission. All the films show the transparency and good adherence to the substrate. The film deposited at the substrate temperature ($T_S=350^0$C) shows an optical transmittance above 74% in the visible region with a steeper optical absorption curve, which indicates a relatively better crystallinity and lower defect density near the band edge.

The optical band gaps computed from the above relation are estimated to be 2.38, 2.10 and 2.35 eV for films obtained at substrate temperature of 250, 350 and 450^0C, respectively. It is found that the band gap energy is decreased from 2.38 eV to 2.10 eV as the deposition temperature was increased from 250^0C to 350^0C. This behavior indicates that when the substrate temperature was increased, the band gap shifted to a lower energy value with the increase in deposition temperature and transmittance. As a result, the band gap of crystallites decreases with increasing substrate temperature, which indicates that crystallization, would cause the E_g narrowing. It could be explained by crystalline state improvement with increasing the substrate temperature.

The crystallization of the CuS films increases with the annealing temperature. It may be due to reduction in the grain boundary scattering, when crystalline size

increases, which supports the XRD results. As the thickness increases, the band gap energy decreases, which may be attributed due to grain growth and increase of localized grain boundary, which in turn increases the point defects. The most important influence of the annealing process on the optical characteristics is related to recrystallization of the CuS crystallites. Changes in the bandgap energy with annealing temperature can be associated to changes in the lattice parameter, induced strains due to thermal expansion and to size growth of the crystallites. The bandgap energy decreases when the lattice parameter decreases when the size of the crystallites increases. And also the decreased band gap after annealing is due to the improvement in the crystalline nature of the material.

The corresponding values of optical energy gap E_g are found to decrease with the annealing treatment due to the improved crystallization of the films, can be attributed to an increase in the of thermally induced crystalline phase. Therefore, there are two possibilities to improve the crystallinity of the films; the increase of the grain size to decrease the number of grain boundaries; the decrease of the barrier height at the grain boundaries.

REFERANCES

[1] Cruz-Vasquez, C., Inoue, M., Inoue, M.B., Bernal, R. and Espinoza-Beltran, F.J. (1999). Characterization of New Copper Suphide Materials. *Superficies y Vacio*, **9**, 219-221

[2] Li, D., Bancroft, G. M., Kasrai, M., Fleet, M. E., Feng, X. H., Yang, B. X. and Tan, K. H. (1994). S K- and L-edge XANES and Electronic Structure of Some Copper Sulfide Minerals. *Phys. Chem. Minerals*, **21** (5), 317-324

[3] Fernandez, A. M., Sebastian, P. J., Campos, J., Gomez-Daza, O., Nair, P. K. and Nair, M. T. S. (1994). Structural and Opto-Electronic Properties of Chemically Deposited Cu$_x$S Thin Film and the Precipitate. *Thin Solid Films*, **237**, 141-147

[4] Isac, L. A., Duta, A., Kriza, A., I A Enesca,I.A. and Nanu, M. (2007). The growth of CuS Thin Films by Spray Pyrolysis. *Journal of Physics: Conference Series*, **61**, 2477

[5] Podder, J., Kobayashi, R. and Ichimura, M. (2005). The Growth of CuS Thin Films by Spray Pyrolysis. *Thin Solid Films*, **61**, 427

[6] Nomura, R., Miyawaki, K., Toyosaki, T. and Matsuda, H. (1996). Preparation of Copper Sulfide Thin Layers by a Single-Source MOCVD Process. *Chemical Vapor Deposition*, **2**, 174-179

[7] Isac, L., Enesca, A., Volmer, M., Duta, A. and Brezeanu, M. (2005). *Proc. Int. Conf. on Materials Science and Engineering BRAMAT*. Brasov Transilvania University Publishing House, Romania.

[8] (a) Nascu, H. and Popescu, V. (2003). *Proc. Int. Conf. on Materials Science and Engineering BRAMAT*. Brasov Transilvania University Publishing House, Romania. (b) Madarasz, J., Okuya, M. and Kaneko, S. (2001). *Journal of European Ceramic Society*, Elsevier, UK.

(c) Isac, L., Duta, A., Kriza, A., Nanu, M., Dumitrescu, L. and Schoonman, J. (2006). *Proc. 7th Int. Conf. on Technology and Quality for Sustained Development TQSD*. AGIR Publishing House, Bucharest Romania.

[9] Ezema, F. I., Hile, D. D., Ezugwu, S. C., Osuji, R. U. and Asogwa, P. U. (2010). Optical Properties of CdS/CuS & CuS/CdS Heterojunction Thin Films Deposited by Chemical Bath Deposition Technique. *Journal of Ovonic Research*, **6** (3), 99-104

[10] Wang, Sheng-Yue, Wang, Wei and Lu, Zu-Hong (2003). Asynchronous-Pulse Ultrasonic Spray Pyrolysis Deposition Of Cu_xS (X=1,2) Thin Films. *Materials Science and Engineering*, **103**, 184-188

[11] Nagcu, C. , Pop, I. , Ionescu, V. , Indrea E. and Bratu I. (1997). Spray Pyrolysis Deposition of CuS Thin Films. *Materials Letters*, **32**, 73-77

[12] Nair, M. T. S., and Nair, P. K. (1989). Chemical Bath Deposition of Cu_xS Thin Films and Their Prospective Large Area Applications. *Semiconductor Science Technology*, **4**, 191

[13] Nair, P. K., Nair, M. T. S., and Campos, J. (1987). In: CM Lampert. *Proc. SPIE*, **823**, 256

[14] Nair, P. K., Nair, M. T. S., Campos, J. and Sansorex, L. E. (1987). A Critical Discussion of the Very High Photoconductivity in Chemically Deposited Cadmium Sulfide Thin Films: Implications for Solar Cell Technology. *Solar Cells*, **22**, 211-227

[15] Nair, P. K., Campos, J. and Nair, M. T. S. (1988). Opto-Electronic Characteristics of Chemically Deposited Cadmium Sulphide Thin Films. *Semiconductor Science Technology*, **3**, 134

[16] Nair, P. K. and Nair, M. T. S. (1987). Prospects of Chemically Deposited CdS Thin Films in Solar Cell Applications. *Solar Cells*, **22**, 103-112

[17] Sebastian, P. J., Gomez-Daza, O., Campos, J., Banos, L. and Nair, P. K. (1994). The Structural, Transport and Optical Properties of Screen Printed Cu_xS Thick Films. *Solar Energy Materials and Solar Cells*, **32**, 159-168

[18] Varkey, A. J. (1990). Prospects for Solution-Grown Cu_2S And Ag_2S Thin Films in Photovoltaic and Architectural Applications. *lnternational Journal of Materials and Product Technology*, **5**, 264-272

[19] Cumberbatch, T. J. and Parden, P. E. (1986). *E.C. Photovoltaic Sol. Energy Conference*, **7**, 675

[20] Gadgil, S. B., Thangaraj, R., lyer, J. V., Sharma, A. K., Gupta, B. K. and Agnihotri, O. P. (1981). Spectrally Selective Copper Sulphide Coatings. *Solar Energy Materials*, **5**, 129

[21] Mattox, D. M. and Sowell, R. R. (1974). High Absorptivity Solar Absorbing Coatings. *Journal of Vacuum Science Technology*, **11**, 793-796

[22] Pillai, P. K. C. and Agarwal, R. C. (1980). Preparation and Characterisation of a Spectrally Selective Black Chrome Coating for Solar Energy Applications. *Applied Energy*, **7** (4), 299-303

[23] Nair, P. K. and Nair, M. T. S. (1991). Chemically Deposited SnS-Cu_xS Thin Films with High Solar Absorptance: New Approach to All-Glass Tubular Solar Collectors. *Journal of Physics D: Apply Physics*, **24**, 83

[24] Nair, P. K., Garcia, V. M., Fernandez, A. M., Ruiz, H. S. and Nair, M. T. S. (1991). Optimization of Chemically Deposited Cu_xS Solar Control Coatings. *Journal of Physics D: Apply Physics*, **24**, 441

[25] Nair, M. T. S. and Nair, P. K. (1991). SnS-Cu_xS Thin Film Combination: A Desirable Solar Control Coating for Architectural and Automobile Glazings. *Journal of Physics D: Apply Physics*, **24**, 450

[26] Nair, M. T. S., Alvarez-Garcia, G., Estrada-Gasca C. A. and Nair, P. K. (1993). Chemically Deposited Bi_2S_3-Cu_xS Solar Control Coatings. *Journal Electrochemical Society*, **140**, 212

[27] Nair, P. K., Nair, M. T. S., Pathirana, H. M. K., Zingaro, R. A. and Meyers, E. A. (1993). Structure and Composition of Chemically Deposited Thin Films of Bismuth Sulfide and Copper Sulfide. *Journal Electrochemical Society*, **140**, 754

[28] Nair, P. K., Nair, M. T. S., Fernandez, A. M. and Ocampo, M. (1989). Prospects of Chemically Deposited Metal Chalcogenide Thin Films for Solar Control Applications. *Journal of Physics D: Apply Physics*, **22**, 829

[29] Yamamoto, T., Kubota, E., Taniguchi, A., Dev, S., Tanaka, K. and Osakada, K. (1992). Electrically Conductive Metal Sulfide-Polymer Composites Prepared by Using Organosols of Metal Sulfides. *Chemistry of Materials*, **4** (3), 570-576

[30] Hudson, M. J. and Galer, J. M. (1994). Synthesis and Characterisation of Conducting Copper Sulphide Surfaces on Textile Fibres: Part 2. *Solid State Ionics*, **73**, 175-183

[31] Grozdanov, I. (1994). Electroconductive Copper Selenide Films on Transparent Polyester Sheets. *Synthetic Metals*, **63**, 213-216

[32] Grozdanov, I., Barlingay, C. K., Dey, S. K., Ristov, M. and Najdoski, M. (1994). Experimental Study of the Copper Thiosulfate System with Respect to Thin-Film Deposition. *Thin Solid Films*, **250**, 67-71

[33] Yamamoto, T., Tanaka, K., Kubota, E. and Osakada, S. (1993). Deposition of Copper Sulfide on the Surface of Poly (Ethylene Terephthalate) and Poly (Vinyl Alcohol) Films in Aqueous Solution to Give Electrically Conductive Films. *Chemistry of Materials*, **5** (9), 1352-1357

[34] Inoue, M., Cruz-Vazquez, C., Inoue, M. B. and Fernando, Q. (1992). Electroconducting Transparent Film of Amorphous Copper Sulfide on Polyethylene Substrate. *Journal of Materials Chemistry*, **2**, 761-762

[35] Im, S. S., Im, H. S. and Kang E.Y. (1990). The Electrical and Physical Properties of CuS- and CdS-Polyacrylonitrile Composite Films Prepared by Using the Organosol Method. *Journal of Applied Polymer Science*, **41**, 1517-1531

[36] Nacu, C., Pop, I., Ionescu, V., Indrea, E. and Bratu, I. (1997). Spray Pyrolysis Deposition of CuS Thin Films. *Materials Letters*, **32**, 73-77

[37] Im, S. S., Lee, J. S. and Kang, E. Y. (1992). Preparation and Electrical Properties of Metal Sulfides-Amidoximated PAN Composite Film. *Journal of Applied Polymer Science*, **45**, 827-836

[38] Thongtem, S., Wichasilp, C. and Thongtem, T. (2009). Transient Solid-State Production of Nanostructured CuS Flowers. *Materials Letters*, **63**, 2409-2412

[39] Thongtem, S., Wichasilp, C. and Thongtem, T. (2009). Transient Solid-State Production of Nanostructured CuS Flowers. *Materials Letters*, **63** (28), 2409-2412

[40] Zhang J. and Zhang, Z. (2008). Hydrothermal Synthesis and Optical Properties of CuS Nanoplates. *Materials Letters*, **62**, 2279-2281

[41] Zhang, P. and Gao, L. (2003). Copper Sulfide Flakes and Nanodisks. *Journals of Materials Chemistry*, **13**, 2007-2010

[42] Thongtem, T., Phuruangrat, A. and Thongtem, S. (2010). Characterization of Copper Sulfide Nanostructured Spheres and Nanotubes Synthesized by Microwave-assisted Solvothermal Method. *Materials Letters*, **64**, 136-139

[43] Ratanatawanate, C., Bui, A., Vu, K. and Balkus, K. J. (2011). Low-Temperature Synthesis of Copper(II) Sulfide Quantum Dot Decorated TiO_2 Nanotubes and Their Photocatalytic Properties. The *Journal of Physical Chemistry C*, **115** (14), 6175-6180

[44] Thongtem, T., Phuruangrat, A. and Thongtem, S. (2007). Synthesis and Analysis of CuS with Different Morphologies Using Cyclic Microwave Irradiation. *Journal of Materials Science*, **42**, 9316-9323

[45] Castillon-Barraza, F. F., Farias, M. H., Coronado-Lopez, J. H., Encinas-Romero, M. A., Perez-Tello, M., Herrera-Urbina, R. and Posada-Amarillas, A. (2011). Synthesis and Characterization of Copper Sulfide Nanoparticles Obtained by the Polyol Method. *Advanced Science Letters*, **4** (2), 596-601

[46] Uppal, P. N. and Burton, L. C. (1983). X-Ray and XPS Studies of Evaporated Cu_xS Thin Films. *Journal of Vacuum Science & Technology A: Vacuum, Surfaces, and Films*, **1** (2), 479-482

[47] Li, F., Kong, T., Bi, W., Li, D., Li, Z. and Huang, X. (2009). Synthesis and Optical Properties of CuS Nanoplate-Based Architectures by a Solvothermal Method. *Applied Surface Science*, **255**, 6285-6289

[48] Neville, R. C. (1995). *Solar Energy Conversion: The Solar Cell*. Elsevier, Amsterdam.

[49] Najdoski, M. Z., Grozdanov, I. S., Dey, S. K. and Siracevska, B. B. (1998). Chemical Bath Deposition of Mercury(II) Sulfide Thin Layers. *Journal of Materials Chemistry*, **8**, 2213-2215

[50] Zhao, F., Chen, X., Xu, N., Lu, P., Zheng, J., Su, Q. and Wu, M. (2006). Controlled Growth of Cu_2S Hexagonal Microdisks and Their Optical Properties. *Journal of Physics and Chemistry of Solids*, **67**, 1786-1791

[51] Joachim, C. and Roth, S. (1997). *Atomic and Molecular Wires*. Kluwer Academic Publishers, London.

[52] Gorai, S., Ganguli, D. and Chaudhuri, S. (2005). Shape Selective Solvothermal Synthesis of Copper Sulphides: Role of Ethylenediamine-Water Solvent System. *Materials Science and Engineering B*, **116** (2), 221-225

[53] Iijima, S. (1991). Helical Microtubules of Graphitic Carbon. *Letters to Nature*, **354**, 56-58

[54] Martin, C. R. (1994). Nanomaterials: A Membrane-Based Synthetic Approach. *Science*, **266**, 1961-1966

[55] Sun, S. H., Meng, G. W., Wang, Y. W., Gao, T., Zhang, M. G., Tian, Y. T., Peng, X. S. and Zhang, L. D. (2002). Large-scale Synthesis of SnO_2 Nanobelts. *Applied Physics A: Materials Science & Processing*, **76** (2), 287-289

[56] Dong, C. L., Mattesini, M., Augustsson, A., Wen, X. G., Zhang, W. X., Yang, S. H., Persson, C., Ahuja, R., Luning, J., Chang, C. L. and Guo, J. H. (2006). Electronic Structure and Surface Structure of Cu_2S Nanorods from Polarization Dependent X-Ray Absorption Spectroscopy. *Journal of Electron Spectroscopy and Related Phenomena*, **151**, 64-70

[57] Wilcox Sr., D. L., Berg, M., Bernat, T., Kellerman, D. and Cochran Jr., J. K. (1995), Hollow and Solid Spheres and Microspheres Science and Technology Associated with their Fabrication and Application. *Materials Research Society Proceedings*, **372**

[58] Ni, Y., Wang, F., Liu, H., Liang, Y., Yin, G., Hong, J., Ma, X. and Xu, Z. (2003). Fabrication and Characterization of Hollow Cuprous Sulfide ($Cu_{2x}S$) Microspheres by a Simple Template-Free Route. *Inorganic Chemistry Communications*, **6**, 1406-1408

[59] Shur, M. S. (2002). Semiconductor Thin Films and Thin Film Devices for Electrotextiles. *Proc.Workshop on Frontiers in Electronics*, **12** (2), 371-390

[60] Pala, N., Rumyantsev, S. L., Sinius, J., Talapatra, S., Shur, M. S. and Gaska, R. (2004). CuS Thin Films on Flexible Substrates. *Electronics Letters*, **40** (4)

[61] Lumelsky, V., Shur, M. S., and Wagner, S. (World Scientific, 2000). (Eds): 'Sensitive Skin'. Also published as Special Issue, *Int. J. High Speed Electron. Syst.*, **10** (2)

[62] Shur, M. S. (2002). Structural and Transport Properties of CdS Films Deposited on Flexible Substrates, *Solid-State Electronics*, **46** (9), 417-420

[63] Sinius, J., Gaska, R., and Shur, M. S. (2000). Flexible Semiconductor Films for Sensitive Skin. Proc. 2000 IEEE=RSJ Int. Conf. on Intelligent Robots and Systems. Takamatsu, Japan, **2**, 1511-1515

[64] Shur, M. S., et al. (2001). Photovoltaic Effect in CdS on Flexible Substrate. *Electronics Letters*, **37** (8), 518-519

[65] Shur, M. S., et al. (2001). Photovoltaic-Effect in Threads Covered with CdS. *Electronics Letters*, **37** (16), 1036-1038

[66] Sinius, J., Gaska, R., and Shur, M. S. (2000). *Flexible Semiconductor Films for Sensitive Skin. Proc. IROS2000*. Kagawa University, Takamatsu, Japan.

[67] Yildirim, M. A., Ates, A. and Astam, A. (2009). Annealing and Light Effect on Structural, Optical and Electrical Properties of CuS, CuZnS and ZnS Thin Films Grown by the SILAR Method. *Physica E*, **41**, 1365-1372

[68] Nair, M. T. S. and Nair, P. K. (1989). Chemical Bath Deposition of Cu_xS Thin Films and Their Prospective Large Area Applications. *Semiconductor Science Technology*, **4**, 191-199

[69] Massa, Werner (2004). *Crystal Structure Determination*. Sprinter-Verlog, Germany, p.1.

[70] Grundmann, Marius (2006). *The Physics of Semiconductors*. Springer-Verlog, Germany , p. 29.

[71] Grahn, Holger T. (2001). *Introduction to Semiconductor Physics*. Uto-Print, Singapore.

[72] Hyde, F. J. (1965). *Semiconductors*. Macdonald, London, p. 44.

[73] Li, Sheng (2006). *Semiconductor Physical Electronics*. Spinger, USA.

[74] Parker, Greg (1994). *Introductory Semiconductor Device Physics*. Prentice-Hall Press, New York.

[75] Wang, Shyh (1989). *Fundamentals of Semiconductor Theory and Device Physics*. Prentice-Hall Press, USA, p. 192.

[76] Tooley, M. H., Tooley, M. and Wyatt, D. (2009). *Aircraft Electrical and Electronic Systems*. Elsevier Ltd., USA, p. 35.

[77] Harper, Charles A. (2002). *Electronic Assembly Fabrication: Chips, Circuit Boards, Packages and Components*. McGraw-Hill, USA.

[78] Phillips, J. C. (1973). *Bonds and Bands in Semiconductors*. Academic Press, London, p.1.

[79] Boer, Karl Wolfgang (1990). *Survey of Semiconductor Physics*. Van Nostrand Reinhold, New York, p.1.

[80] Neamen, Donald A. (2003). *Semiconductor physics and devices*. McGraw-Hill, Boston.

[81] Suchet, J.P. (1975). *Electrical Conduction in Solid Materials*. Pergamon Press, Great Britain.

[82] Balandin, A. A. and Wang, K. L. (2006). *Handbook of Semiconductor Nanostructures and Nanodevices*. American Scientific Publishers, USA.

[83] Muller, Richard S. and Kamins, Theodore I. (1986). *Device Electronics for Integrated Circuits*. New York.

[84] Yu, Peter Y. and Cardona, Manual (2004). *Fundamental of Semiconductors: Physics and Materials Properties*. Springer Press, USA.

[85] Parker, Greg, Introductory Semiconductor Device Physics, Prentice Hall, New York, 1994.

[86] Khan, Anwar A.& Dey and Kanchan K. (2006). *A First Course in Electronics*. Prentice-Hall, New Delhi, ISBN-81-203-2776-4.

[87] Colinge, Jean-Pierre and Colinge, A. Cynthia (2002). *Physics of Semiconductor Devices*, USA.

[88] Turley, Jim (2002). *The Essential Guide to Semiconductors*. Prentice Hall PTR, New Jersey.

[89] Sze, S. M. (1969). *Physics of the Semiconductor Device*. Murray Hill, New Jersey.

[90] Bedir, M., Öztaş, M., Bakkaloğlu, Ö. F. and Ormancı, R. (2005). Investigations on Structural, Optical and Electrical Parameters of Spray Deposited ZnSe Thin Films with Different Substrate Temperature. *The European Physical Journal B*, **45**, 465-471